Multi-phase structural optimization via a level set method

Grégoire Allaire, Charles Dapogny, Gabriel Delgado, Georgios Michailidis

MULTI-PHASE STRUCTURAL OPTIMIZATION VIA A LEVEL SET METHOD

G. ALLAIRE[1], C. DAPOGNY[2,3], G. DELGADO[1,4], G. MICHAILIDIS [1,3]

[1] *CMAP, Ecole Polytechnique, 91128 Palaiseau.*
[2] *UPMC Univ Paris 06, UMR 7598, Laboratoire J.-L. Lions, F-75005 Paris, France.*
[3] *Renault DREAM-DELT'A Guyancourt, France.*
[4] *EADS Innovation Works, Suresnes, France.*

ABSTRACT. We consider the optimal distribution of several elastic materials in a fixed working domain. In order to optimize both the geometry and topology of the mixture we rely on the level set method for the description of the interfaces between the different phases. We discuss various approaches, based on Hadamard method of boundary variations, for computing shape derivatives which are the key ingredients for a steepest descent algorithm. The shape gradient obtained for a sharp interface involves jump of discontinuous quantities at the interface which are difficult to numerically evaluate. Therefore we suggest an alternative smoothed interface approach which yields more convenient shape derivatives. We rely on the signed distance function and we enforce a fixed width of the transition layer around the interface (a crucial property in order to avoid increasing "grey" regions of fictitious materials). It turns out that the optimization of a diffuse interface has its own interest in material science, for example to optimize functionally graded materials. Several 2-d examples of compliance minimization are numerically tested which allow us to compare the shape derivatives obtained in the sharp or smoothed interface cases.

Key words: Shape and topology optimization, multi-materials, signed distance function.

1. INTRODUCTION

Structural optimization has dragged the interest of an increasing number of engineers during the last decades. It provides valuable help in problems where mechanical intuition is limited. One instance of such a problem, which is of great relevance in material science and industry, is to find the optimal distribution of several materials in a fixed working domain, in order to minimize a criterion related to the overall mechanical behavior or cost of the phases mixture.

A crucial issue in the modeling of this problem is the parametrization of the phases mixture. While the exact formulation require the material properties, or the global Hooke's tensor, to be discontinuous at the interfaces between two materials, it is often convenient, for numerical purposes, to devise an appropriate interpolation scheme to smooth the coefficients or equivalently to replace sharp interfaces by diffuse ones. This diffuse or smeared interface approach has its own interest when one is interested in the optimization of functionally graded materials [9], [26], [43], [46], [47].

There is already a vast literature about multiphase optimization and various methods have been proposed to address the problem. The Hadamard method of geometric shape optimization, as described in [17], [23], [32], was used, for example, in [22] for optimal composite design. The homogenization method [1], [13], [45] was the main tool in the multiphase problem studied in [3] for the optimal reloading of nuclear reactors (sequential laminates were shown to be optimal composite materials). In the framework of the SIMP (Solid Isotropic Material with Penalization) method, several interpolation schemes have been proposed for the mathematical formulation of the Hooke's tensor of the mixture [7], [44], [52]. In general, material interpolation schemes can be quite involved [52] and one may design such a model in order to favor certain phases [44]. Applications range from the design of materials with extreme or unusual thermal expansion behavior [40] to multi-material actuators [41], through conductivity optimization for multi-phase microstructural materials [54]. In the framework of the phase-field method, a generalized Cahn-Hilliard model of multiphase transition was implemented in [53] to perform multimaterial structural optimization.

The first publications on multiphase optimization, using the level set method, are [29] and [50] (see also [30], [49], [51]). Following an idea of Vese and Chan [48], the authors in [29], [50] used m level set functions to represent up to $n = 2^m$ materials: we shall adhere to this setting (see section 4). The level

set functions are advected through eikonal Hamilton-Jacobi equations in which the normal velocity is given by the shape derivative of the objective function. Unfortunately, the shape derivatives, derived in [29] and [50], are not correct in full mathematical rigor as we explain in section 5. Fortunately, these shape derivatives are approximations of the correct formula upon various assumptions. A first goal of the present paper is to clarify the issue of shape differentiability of a multiphase optimization problem. In section 2 we give the correct shape derivative in the setting of a sharp interface between phases (see Proposition 2.2). It was first obtained in [5] for a problem of damage and fracture propagation but, in a scalar setting, previous contributions can be found in [24], [8], [37]. Because the phase properties are discontinuous through the interfaces, the transmission conditions imply that only the elastic displacement and the normal stress are continuous at the interfaces, leaving the tangential stress and the normal strain discontinuous. These discontinuities yield obvious difficulties which must be handled carefully. The exact or continuous shape derivative turns out to be somehow inadequate for numerical purposes since it involves jumps of strains and stresses through the interfaces, quantities which are notably hard to evaluate with continuous finite elements. Therefore, Proposition 2.5 gives a discrete variant of this shape derivative which does not involve any jumps and is similar to the result of [29] and [50]. The idea is to consider a finite element approximation of the elasticity system, the solution of which has no derivative jumps through the interface, implying that the shape derivative is much easier to compute.

Another delicate issue in multiphase optimization using the level set method is that the interface is inevitably diffused and its thickness may increase, thus deteriorating the peformance of the analysis and eventually of the optimization. Note that, for most objective functions, it is always advantageous to introduce intermediate values of the material properties, so that the interface spreading is produced by the optimization process itself and not merely by the numerical diffusion. In [29] the authors introduced a penalization term to control the width of the interpolation zone between the materials. In [50] the level set functions are re-initialized to become signed distance functions, which permits a more explicit control of the interpolation width. A second goal of the present paper is to propose a smoothed interface setting which guarantees a fixed thickness of the interface without any increase in its width (as it is already the case in the standard single material level set method for shape and topology optimization). In section 3 we describe a regularization of the interface which relies on the signed distance function to the interface. Note that the signed distance function has nothing to do with the level set function which is used in numerical simulations. Indeed, the solution of the advection Hamilton-Jacobi equation (with a velocity given by the shape derivative) is usually not the signed distance function (which explains why reinitialization is often used in practice). In such a smoothed interface setting our main result is Theorem 3.14 which gives the shape derivative of the objective function. It requires several intermediate technical results, notably finding the shape derivative of the distance function (first obtained in [18]) and using a coarea formula to reduce a volume integral to a product integral on the interface and along normal rays. Once again, we show in section 3.5 that, when the regularization parameter (or the thickness of the diffuse interface) is vanishingly small, the exact shape derivative can be approximated by the formula already obtained in Proposition 2.5 which corresponds to the result of [29] and [50] too.

Section 3.6 explains how the smoothed interface model converges to the sharp interface problem as the regularization parameter goes to zero. Since, for simplicity, all the previous theoretical results were stated in the case of a single interface between two phases, we explain how to generalize our smoothed interface setting to more materials in section 4. Section 5 is devoted to a comparison with [29] and [50]. Finally, in section 6 we show several 2-d results and make comparisons between the different settings and formulas for the shape derivatives. Some optimal designs obtained by our approach are compared to those previously computed in [50] and [51]: ours are more symmetric and sometimes slightly different. We believe it is due to our use of a correct shape derivative instead of an approximate one.

2. Sharp-interface formulation in a fixed mesh framework

To simplify the exposition in the first sections we limit ourselves to the case of two materials. Of course, the proposed approach extends to more phases and the corresponding details are given in section 4.

2.1. **Description of the problem.**

The general purpose of this paper is to optimize the position of the interface Γ between two linear elastic materials, hereafter labeled as 0 and 1, with respective Hooke's law A_0, A_1. These materials fill two respective subdomains Ω^0, Ω^1 of a (bounded) working domain D of $\mathbb{R}^d$, ($d = 2$ or 3) which accounts for the resulting structure of the optimal distribution of materials, i.e. $D = \Omega^0 \cup \Gamma \cup \Omega^1$. To avoid mathematical technicalities, we assume that Γ is a smooth surface without boundary and strictly included in D, that is, $\Gamma \cap \partial D = \emptyset$. We refer to Ω^1 as the *exterior* subdomain, so that $\partial \Omega^0 = \Gamma$ (see Figure 1). Thus, the shape of the interface Γ is altogether conditionned by that of Ω^0, and conversely. In the sequel, the variable of shape optimization is denoted either by Γ or Ω^0, without distinction.
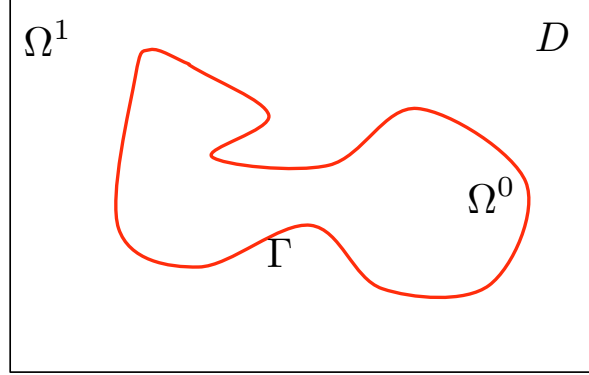

FIGURE 1. Fixed working domain D occupied by two distinct materials Ω^0 and Ω^1 separated by a smooth interface Γ.

The structure D is clamped on a part $\Gamma_D \subset \partial D$ of its boundary, and is submitted to *body forces* and *surface loads*, to be applied on a part $\Gamma_N \subset \partial D$, which are given as two vector-valued functions defined on D, respectively $f \in L^2(D)^d$, and $g \in H^1(D)^d$.

Perhaps the most natural and physical way to model such a distribution of two materials among a fixed working domain is the so-called *sharp-interface formulation*. More specifically, the total Hooke's law on D is defined as $A_\chi := A_0 \chi_0 + A_1 \chi_1$, where χ_i stands for the characteristic function of the phase Ω^i. In this context, the *displacement field* u is the unique solution in $H^1(D)^d$ to the linearized elasticity system

(1)
$$\begin{cases} -\operatorname{div}(A_\chi\, e(u)) &=& f & \text{in } D \\ u &=& 0 & \text{on } \Gamma_D \\ (A_1\, e(u)) \cdot n &=& g & \text{on } \Gamma_N, \end{cases}$$

where $e(u) = \frac{{}^t \nabla u + \nabla u}{2}$ is the strain tensor, and n stands for the outer unit normal vector to ∂D.

Our purpose is to minimize an objective function of the interface Γ, which is rather expressed as a function $J(\Omega^0)$ of the interior subdomain,

(2)
$$J(\Omega^0) = \int_D j(x, u)\, dx + \int_{\Gamma_N} k(x, u)\, ds,$$

where $j(x, u)$ and $k(x, u)$ are smooth functions satisfying adequate growth conditions. A typical example is the *compliance* of the structure D (the work done by the loads), which reads

(3)
$$J(\Omega^0) = \int_D f \cdot u\, dx + \int_{\Gamma_N} g \cdot u\, ds = \int_D A_\chi(x) e(u) : e(u) dx.$$

Of course, the minimization of (2) or (3) is complemented by a volume constraint on the phase A_0. In particular, it is often a requirement in order to avoid obvious designs made of only one phase.

We do not discuss the well-posedness of this optimal design problem. Let us simply recall that the minimization of (2) or (3) usually does not admit a solution in the class of open subsets $\Omega_0 \subset D$. Existence of an

optimal shape is rather obtained with some additional smoothness or geometrical or topological constraints (for example, imposing a uniform bound on the perimeter of Ω_0, i.e., on the measure of the interface Γ).

2.2. Shape-sensitivity analysis of the sharp-interface problem.

There exists a vast literature on the Hadamard method for computing derivatives with respect to the exterior boundary (see e.g. [2], [17], [23], [32] and references therein) but relatively few works on the derivation with respect to an interface between two regions. In the conductivity context (i.e. replacing (1) by a scalar equation), derivatives with respect to an interface have been obtained in [24], [8], [37]. These results were extended to the elasticity setting in [5]. Let us also mention the works [25], [34] where similar results are obtained for a stratified media (where the interfaces are flat and parametrized by a single scalar parameter).

We briefly recall the definition of shape differentiation in the present context of interface variations. For a smooth open subset $\Omega^0 \subset D$, we consider variations of the type

$$\left(Id + \theta\right)(\Omega^0) := \left\{x + \theta(x) \text{ for } x \in \Omega^0\right\},$$

with $\theta \in W^{1,\infty}(D; \mathbb{R}^d)$ such that θ is tangential on ∂D (this last condition ensures that $D = (Id + \theta)D$). It is well known that, for sufficiently small θ, $(Id + \theta)$ is a diffeomorphism in D.

Definition 2.1. The shape derivative of a function $J(\Omega^0)$ is defined as the Fréchet derivative in $W^{1,\infty}(D; \mathbb{R}^d)$ at 0 of the application $\theta \to J\left((Id + \theta)\Omega^0\right)$, i.e.

$$J\left((Id + \theta)\Omega^0\right) = J(\Omega^0) + J'(\Omega^0)(\theta) + o(\theta) \quad \text{with} \quad \lim_{\theta \to 0} \frac{|o(\theta)|}{\|\theta\|_{W^{1,\infty}}} = 0 \,,$$

where $J'(\Omega^0)$ is a continuous linear form on $W^{1,\infty}(D; \mathbb{R}^d)$.

As noticed in [5] and [37], the essential ingredients that must be considered in the calculation of the shape derivative of a problem such as (1) are the transmission conditions and the differentiability of the solution u with respect to the interface Γ. Furthermore, when a numerical implementation is sought, an additional element must be taken into account: the way in which the transmission conditions (continuity of the displacement and continuity of the normal stress across the interface) are interpreted by finite element methods in a fixed mesh framework. In general these methods either partially preserve the transmission conditions (e.g. classical Lagrange finite elements method) or exactly preserve the transmission conditions (e.g. extended finite elements XFEM [42], adapted interface meshing [14], etc.).

It is known [5], [37] that the solution $u \in H^1(D)$ of (1) is not shape differentiable with respect to the interface Γ. The reason is that some spatial derivatives of u are discontinuous across the interface because of the jump of the material elastic properties. Note however that the transported (or pull-back) function $u_\theta := u \circ (Id + \theta)$ is indeed differentiable with respect to θ (this is the difference between the material derivative in the latter case and the shape derivative in the former case, see [2], [23]). It is not necessary to use the concept of material derivative for computing the shape derivative of the objective function. One can stay in a Eulerian framework and use Céa's formal Lagrangian method [11] to find the correct formula for the shape derivative $J'(\Omega^0)(\theta)$. In order to circumvent the non-differentiability of u, the idea is to introduce the restrictions of u on Ω^0 and Ω^1, denoted by $u^0 := u|_{\Omega^0}$ and $u^1 := u|_{\Omega^1}$.

We recall the result of [5] for the shape derivation of the objective function (2). We need to introduce some notations about jumps through the interface Γ. For any quantity s which is discontinuous across Γ, taking values s^0 (resp. s^1) on Ω^0 (resp. Ω^1), denote as $[s] = s^1 - s^0$ the *jump* of s. We also introduce at each point of Γ the local basis obtained by gathering the unit normal vector n (pointing outward Ω^0) and a collection of of unit tangential vectors, denoted by τ, such that (τ, n) is an orthonormal frame. For a symmetric $d \times d$ matrix $\mathcal{M}$, written in this basis, we introduce the notation

$$\mathcal{M} = \begin{pmatrix} \mathcal{M}_{\tau\tau} & \mathcal{M}_{\tau n} \\ \mathcal{M}_{n\tau} & \mathcal{M}_{nn} \end{pmatrix}$$

where $\mathcal{M}_{\tau\tau}$ stands for the $(d-1) \times (d-1)$ minor of $\mathcal{M}$, $\mathcal{M}_{\tau n}$ is the vector of the $(n-1)$ first components of the n-th column of $\mathcal{M}$, $\mathcal{M}_{n\tau}$ is the row vector of the $(n-1)$ first components of the n-th row of $\mathcal{M}$, and $\mathcal{M}_{nn}$ the (n,n) entry of $\mathcal{M}$. Finally, we define the adjoint problem

(4)
$$\begin{cases} -\mathrm{div}\,(A_\chi\,e(p)) &=& -j'(x,u) & \text{in } D, \\ p &=& 0 & \text{on } \Gamma_D, \\ (A_1\,e(p))\cdot n &=& -k'(x,u) & \text{on } \Gamma_N, \end{cases}$$

where the symbol $'$ denotes differentation with respect to u.

Proposition 2.2. The shape derivative of the cost function J, defined in (2), reads

$$J'(\Omega^0)(\theta) = -\int_\Gamma \mathcal{D}(u,p)\,\theta\cdot n\,ds,$$

(5)
$$\mathcal{D}(u,p) = -\sigma(p)_{nn} : [e(u)_{nn}] - 2\sigma(u)_{n\tau} : [e(p)_{n\tau}] + [\sigma(u)_{\tau\tau}] : e(p)_{\tau\tau}.$$

where $[\cdot] = \cdot^1 - \cdot^0$ denotes the jump through Γ, $n = n^0 = -n^1$ and $\sigma(v) = A_\chi\,e(v)$.

Remark 2.3. To better appreciate the expression (5) where some terms have jumps and others not, we recall that the tangential strain tensors $e(u)_{\tau\tau}$ and $e(p)_{\tau\tau}$ are continuous through the interface Γ while the normal components $e(u)_{nn}$, $e(u)_{n\tau}$, $e(p)_{nn}$ and $e(p)_{n\tau}$ are discontinuous. On the contrary, the normal components of the stress tensors $\sigma(u)_{nn}$, $\sigma(u)_{n\tau}$, $\sigma(p)_{nn}$ and $\sigma(p)_{n\tau}$ are continuous through Γ while their tangential parts $\sigma(u)_{\tau\tau}$ and $\sigma(p)_{\tau\tau}$ are discontinuous.

Proof. We merely sketch the proof that can be found in [5]. In order to apply Céa's Lagrangian method [11], we first introduce the restrictions of u on Ω^0 and Ω^1, denoted by $u^0 := u|_{\Omega^0}$ and $u^1 := u|_{\Omega^1}$, which satisfy the transmission problem:

(6)
$$\begin{cases} -\mathrm{div}\,\left(A_1\,e(u^1)\right) &=& f & \text{in } \Omega^1 \\ u^1 &=& 0 & \text{on } \Gamma_D \cap \partial\Omega^1 \\ \left(A_1\,e(u^1)\right)\cdot n &=& g & \text{on } \Gamma_N \cap \partial\Omega^1 \\ u^1 &=& u^0 & \text{on } \Gamma \\ (A_0 e(u^0))\cdot n^0 + (A_1 e(u^1))\cdot n^1 &=& 0 & \text{on } \Gamma, \end{cases}$$

and

(7)
$$\begin{cases} -\mathrm{div}\,\left(A_0\,e(u^0)\right) &=& f & \text{in } \Omega^0 \\ u^1 &=& u^0 & \text{on } \Gamma \\ (A_0 e(u^0))\cdot n^0 + (A_1 e(u^1))\cdot n^1 &=& 0 & \text{on } \Gamma. \end{cases}$$

Of course, (1) and (6)-(7) are equivalent. Note that, by standard regularity theory [28], u is smooth on each subdomain, namely $u^0 \in H^2(\Omega^0)$ and $u^1 \in H^2(\Omega^1)$. Then, we define the Lagrangian

(8)
$$\begin{aligned} \mathcal{L}(\theta, v^1, v^0, q^1, q^0) &=& \sum_{i=0,1}\left(\int_{(Id+\theta)\Omega^i} j(x,v^i)dx + \int_{\Gamma_N} k(x,v^i)ds\right) \\ &+& \sum_{i=0,1}\left(\int_{(Id+\theta)\Omega^i} A_i e(v^i) : e(q^i)dx - \int_{(Id+\theta)\Omega^i} f\cdot q^i dx - \int_{\Gamma_N} g\cdot q^i ds\right) \\ &+& \frac{1}{2}\int_{(Id+\theta)\Gamma}(\sigma^1(v^1) + \sigma^0(v^0))n\cdot(q^1 - q^0)ds \\ &+& \frac{1}{2}\int_{(Id+\theta)\Gamma}(\sigma^1(q^1) + \sigma^0(q^0))n\cdot(v^1 - v^0)ds, \end{aligned}$$

where the last two surface integrals account for the transmission conditions. Differentiating $\mathcal{L}$ with respect to q^1, q^0 yields the state equations (6)-(7), while differentiating with respect to v^1, v^0 leads to the adjoint equation (4). Then a standard, albeit nasty, computation (see [5] for full details) shows that

$$J'(\Omega^0)(\theta) = \frac{\partial\mathcal{L}}{\partial\theta}(0, u^1, u^0, p^1, p^0)(\theta),$$

which yields the result. $\qquad\square$

Remark 2.4. Proposition 2.2 can be extended in several ways. For example, if the integrand j depend on χ, namely if the objective function is

$$J(\Omega^0) = \int_D j_\chi(x,u)dx + \int_{\Gamma_N} k(x,u)ds := \sum_{i=0,1} \int_{\Omega^i} j_i(x,u)dx + \int_{\Gamma_N} k(x,u)dx,$$

we obtain a shape derivative which is

$$J'(\Omega^0)(\theta) = -\int_\Gamma \Big([j_\chi(x,u)] + \mathcal{D}(u,p) \Big)\theta \cdot n\, ds,$$

with the same expression (5) for $\mathcal{D}(u,p)$.

Although formula (5) for the shape derivative makes perfect sense in a continuous setting, its numerical discretization is not obvious. Indeed, (5) involves jumps through the interface which are difficult to evaluate from a numerical point of view if the interface is not exactly meshed. Let us explain the difficulty by making some specific discretization choices, keeping in mind that any other numerical method will feature similar inconvenients. Suppose D is equipped with a conformal simplicial mesh $D_h = \bigcup_{i=1}^N K_i$ with N elements K_i of maximal size h. Let $\Pi_1(D_h)$ and $\Pi_0(D_h)$ be the finite-dimensional spaces of Lagrange $\mathbb{P}^1$, respectively $\mathbb{P}^0$, finite element functions. Define $u_h, p_h \in \Pi_1(D_h)$ the internal approximations of u and p respectively, i.e.,

$$(9) \qquad \int_D A_\chi e(u_h) : e(v_h)\, dx = \int_D f \cdot v_h\, dx + \int_{\Gamma_N} g \cdot v_h\, ds, \quad \forall v_h \in \Pi_1(D_h),$$

and

$$(10) \qquad \int_D A_\chi e(p_h) : e(v_h)\, dx = -\int_D j'(x,u_h) \cdot v_h\, dx - \int_{\Gamma_N} k'(x,u_h) \cdot v_h\, ds, \quad \forall v_h \in \Pi_1(D_h).$$

Since the discrete strain tensors $e(v_h)$ are constant in each cell K_i, we can replace A_χ in the above internal approximate variational formulation by its $\mathbb{P}^0$ interpolate A^* defined by

$$A^*|_K = \rho A^0 + (1-\rho)A^1, \quad \text{with } \rho = \int_K \chi dx.$$

Within this discretized framework the naive evaluation of the jumps in (5) has no meaning. Indeed, consider the generic case of an element K cut in its interior by the interface Γ (see Figure 2). For $\mathbb{P}^1$ Lagrange finite elements the strain tensors $e(v_h)$, for $v_h = u_h, p_h$, are constant in K, thus yielding a zero jump. Similarly, if the stress tensors are evaluated as $\sigma_h = A^*e(v_h)$, they are constant in K and their jump is again zero, leading to a vanishing shape derivative ! There is an alternative formula for the stress tensor which is $\sigma_h = A_\chi e(v_h)$: it yields a non-vanishing jump $[A]e(v_h)$ and the discretization of (5) would be

$$(11) \qquad (\mathcal{D}(u,p))_h = ([A]e(u))_{\tau\tau} : e(p)_{\tau\tau},$$

which is different from the discrete formula (13) by lack of any normal components. On the same token, note that the "exact" continuity of the normal stress through Γ does not hold for $\sigma_h = A_\chi e(v_h)$ with $v_h = u_h, p_h$ since

$$[\sigma_h \cdot n] = ([A]e(v_h)) \cdot n \neq 0.$$

Henceforth some special care is required for the numerical approximation of (5). A complicated process was proposed in [5] for computing the jump of a discontinuous quantity s_h, based on the diffuse interface approximation

$$(12) \qquad [s_h] \approx \Big((1-\chi)s_h - \chi s_h \Big).$$

Notwithstanding this approximation seems to work well when the contrast between the two elastic phases is very large (as is the case in damage or fracture models, see [5]), more general numerical experiences for comparable elastic moduli indicate a much worse behavior of this approximation, up to the point that (5) does not any longer provide a proper descent direction to minimize (2) (see section 6.2).

This difficulty in the numerical evaluation of the shape derivative (5) is just another example of the well-known paradigm "should we differentiate first and then discretize or *vice versa* ?" as already studied in [35].
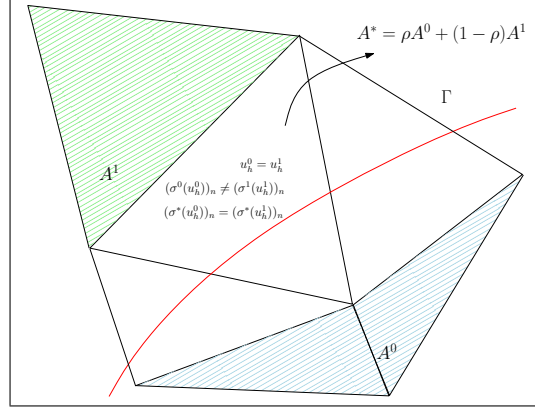
FIGURE 2. Transmission condition in a fixed mesh framework.

In order to circumvate this issue it it tempting, and we do so now, to investigate the case when we first discretize and then differentiate. In other words we consider the objective function

$$J_h(\Omega^0) = \int_D j(x, u_h)\, dx + \int_{\Gamma_N} k(x, u_h)\, ds,$$

where $u_h \in \Pi_1(D_h)$ is the discrete solution of (9).

Proposition 2.5. Assume that the interface Γ generically cut the mesh D_h, namely that it is never aligned with part of a face of any cell K_i. Then, the solution u_h of (9) is shape differentiable and the shape derivative of the cost function J_h is given by

(13)
$$J_h'(\Omega^0)(\theta) = - \int_\Gamma [A_\chi] e(u_h) : e(p_h)\, \theta \cdot n\, ds,$$

where $[\cdot]$ denotes the jump through Γ and p_h is the solution of (10).

Remark 2.6. Note that Proposition 2.5 holds true for most finite elements discretization and not merely $\mathbb{P}^1$ Lagrange finite elements. The assumption on the interface Γ is necessary in the sense that, if a face of an element K of the mesh is embedded in Γ, then neither u_h nor J_h are shape differentiable (in the most favorable case, there would be two directional derivatives corresponding to Γ moving on one side or on the other of this face of K). However, if instead of Lagrange finite elements, we use Hermite finite elements which ensure that $e(u_h)$ is continuous on D, then the results of Proposition 2.5 hold true without any assumption on Γ.

Proof. Let us denote by $\phi_i(x)$ the basis functions of the finite element space $\Pi_1(D_h)$. The solution $u_h \in \Pi_1(D_h)$ is decomposed as

$$u_h(x) = \sum_i U_i^h \phi_i(x),$$

and the vector U^h of components U_i^h is the solution of the linear system

$$K^h U^h = F^h,$$

where the stiffness matrix K^h and the right hand side F^h are defined as

$$K_{i,j}^h = \int_D A_\chi e(\phi_i) : e(\phi_j)\, dx, \text{ and } F_i^h = \int_D f \cdot \phi_i\, dx + \int_{\Gamma_N} g \cdot \phi_i\, ds.$$

The basis functions ϕ_i are independent of Γ so the shape differentiability of the function u_h reduces to that of the vector U^h and thus of the rigidity matrix K^h. Since the quantity $e(\phi_i) : e(\phi_j)$ is piecewise constant on each element K, we need our assumption on Γ which does not overlap any face of K. In such a case we obtain

$$\left(K_{ij}^h\right)'(\Gamma)(\theta) = \int_\Gamma [A_\chi] e(\phi_i) : e(\phi_j)\, \theta \cdot n\, ds$$

7

and thus
$$u'_h(\Gamma)(\theta) = \sum_i \left(U^h_i\right)'(\Gamma)(\theta)\phi_i, \text{ where } \left(U^h\right)'(\Gamma)(\theta) = -(K^h)^{-1}\left(K^h\right)'(\Gamma)(\theta)U^h.$$

Once u_h is shape differentiable, it is not necessary anymore to consider a complicate Lagrangian like (8), taking into account the transmission conditions through Γ (which, by the way, do not hold true for u_h). Therefore we define a discrete Lagrangian as

$$\mathcal{L}_h(\theta, v_h, q_h) = \int_D j(x, v_h)\, dx + \int_{\Gamma_N} k(x, v_h)\, ds + \int_D A_{(Id+\theta)\chi} e(v_h) : e(q_h)\, dx - \int_D f \cdot q_h\, dx - \int_{\Gamma_N} g \cdot q_h\, ds,$$

to which it is easy to apply Céa's method. Note that the adjoint problem obtained by differentiating $\mathcal{L}_h$ with respect to v_h is exactly (10) which was a discretization of the continuous adjoint. Therefore we deduce

$$J'_h(\Omega^0)(\theta) = \frac{\partial \mathcal{L}_h}{\partial \theta}(0, u_h, p_h)(\theta),$$

which yields the desired result. □

There is a clear difference between the discrete derivative (13) and the continuous one (5). Even if the continuous derivative is further discretized as suggested in (11), there is still a difference between (13) and (11) which is that the later one is restricted to the tangential components of the stress and strain tensors.

There is however one case where both formulas coincide which is when one of the phases is void. Indeed, assume that $A_0 = 0$ (and similarly that $f = 0$ and $j = 0$ in Ω^0 so that no loads are applied to the void region). Then, in the domain Ω^0 we have

$$\sigma(p)_{nn} = 0, \ \sigma(p)_{n\tau} = 0, \ \sigma(u)_{nn} = 0 \text{ and } \sigma(u)_{n\tau} = 0.$$

Thus, we deduce that the continuous derivative (5) becomes

$$J'(\Omega^0)(\theta) = -\int_\Gamma \sigma(u^1)_{\tau\tau} : e(p^1)_{\tau\tau}\, \theta \cdot n\, ds,$$

which, upon discretization, coincides with the discrete derivative (13)

$$J'_h(\Omega^0)(\theta) = -\int_\Gamma A^1 e(u_h) : e(p_h)\, \theta \cdot n\, ds,$$

since $\sigma(u^1)_{nn} = \sigma(u^1)_{n\tau} = 0$ on Γ.

The above study shows that the numerical discretization of the sharp-interface problem should be handled carefully when a standard finite element method is used for solving the state and adjoint systems (1) and (4) in a fixed mesh setting. The main reason of this difficulty lies in the difference of regularity of the exact and approximated solutions through the interface. The discrete derivative (13) is very efficient in numerical practice. Many examples are given in [16] in the context of optimal design of laminated composite panels.

3. Shape derivative in the smoothed-interface context

3.1. Description of the problem.

We now present an alternative approach to that of section 2 which can be coined as smoothed or diffuse interface approach. It can be seen as a mathematically convenient approximation of the sharp-interface problem but, as explained in the introduction, it has its own merits for some problems in material science which feature physically thick transition zones [9], [43], [46], [47]. More precisely, either for a mathematical approximation or for physical reasons, it may be desirable to model the interface Γ between Ω^0 and Ω^1 as a thin layer of (small) width $2\varepsilon > 0$ rather than as a sharp interface. In this context, we rely on the notion of *signed distance function.*

Definition 3.1. Let $\Omega \subset \mathbb{R}^d$ be a Lipschitz open set. The *signed distance function* $d_\Omega : \mathbb{R}^d \to \mathbb{R}$ to Ω is defined as

$$(14) \qquad d_\Omega(x) = \begin{cases} -d(x, \partial\Omega) & \text{if } x \in \Omega \\ 0 & \text{if } x \in \partial\Omega \\ d(x, \partial\Omega) & \text{if } x \in {}^c\overline{\Omega} \end{cases},$$

where $d(\cdot, \partial\Omega)$ is the usual Euclidean distance to the boundary $\partial\Omega$.

The material properties in D are defined as a smooth interpolation between A_0 and A_1 in the layer of width 2ε around Γ, so that the resulting Hooke tensor $A_{\Omega^0,\varepsilon}$ reads

$$(15) \qquad A_{\Omega^0,\varepsilon}(x) = A_0 + h_\varepsilon(d_{\Omega^0}(x))(A_1 - A_0), \quad \forall\, x \in D,$$

where $h_\varepsilon : \mathbb{R} \to \mathbb{R}$ is a smooth approximation of the Heaviside function, that is, a smooth monotone function enjoying the properties : $h_\varepsilon(t) = 0$ for $t < -\epsilon$, $h_\varepsilon(t) = 1$ for $t > \epsilon$. In the sequel, we chose the $\mathcal{C}^2$ function

$$(16) \qquad \forall\, t \in \mathbb{R}, \ h_\varepsilon(t) = \begin{cases} 0 & \text{if} \quad t < -\varepsilon \\ \frac{1}{2}\left(1 + \frac{t}{\varepsilon} + \frac{1}{\pi}\sin(\frac{\pi t}{\varepsilon})\right) & \text{if} \quad -\varepsilon \leq t \leq \varepsilon \\ 1 & \text{if} \quad t > \varepsilon \end{cases}$$

Remark 3.2. Formula (16) expresses a simple choice for the interpolation of the material properties between the two materials, and of course, one could think of different interpolation rules. Moreover, the interpolation function could also contain parameters that are themselves subject to optimization (e.g. the layer width ε) and both a geometric and parametric optimization could be combined using a method of alternating directions.

We modify (1) so that the elastic displacement now solves

$$(17) \qquad \begin{cases} -\mathrm{div}\left(A_{\Omega^0,\varepsilon}\, e(u)\right) &=& f & \text{in } D \\ u &=& 0 & \text{on } \Gamma_D \\ (A_1\, e(u)) \cdot n &=& g & \text{on } \Gamma_N. \end{cases}$$

The objective function does not change and we still minimize (2) which depends on d_{Ω^0} through (15). Before we compute its shape derivative, we need to recall some properties of the signed distance function d_{Ω^0}. This is the purpose of the next subsections.

3.2. Shape differentiability of the signed distance function.

The purpose of this section is to recall some results on the signed distance function and to explore its shape differentiability which holds in a non-classical and subtle sense (see below for details). For simplicity we drop the index 0 of Ω^0 in the sequel. For a Lipschitz bounded domain $\Omega \subset D$ we consider shape variations in the sense of Hadamard as in Definition 2.1, i.e., $(Id+\theta)\Omega$, for a (small) vector field $\theta \in W^{1,\infty}(D, \mathbb{R}^d)$.

Let us start by collecting some definitions (see Figure 3 for a geometric illustration).

Definition 3.3. Let $\Omega \subset \mathbb{R}^d$ be a Lipschitz bounded open set.
- For any $x \in \mathbb{R}^d$, $\Pi_{\partial\Omega}(x) := \{y_0 \in \partial\Omega \text{ such that } |x - y_0| = \inf_{y \in \partial\Omega}|x - y|\}$ is the *set of projections* of x on $\partial\Omega$. It is a closed subset of $\partial\Omega$. When $\Pi_{\partial\Omega}(x)$ reduces to a single point, it is called the *projection* $p_{\partial\Omega}(x)$ of x onto $\partial\Omega$.
- $\Sigma := \left\{x \in \mathbb{R}^d \text{ such that } (d_\Omega)^2 \text{ is not differentiable at } x\right\}$ is the *skeleton* of $\partial\Omega$ (or Ω by a small abuse in terminology).
- For any $x \in \partial\Omega$, $\mathrm{ray}_{\partial\Omega}(x) := \{y \in \mathbb{R}^d \text{ such that } d_\Omega \text{ is differentiable at } y \text{ and } p_{\partial\Omega}(y) = x\}$ is the ray emerging from x. Equivalently, $\mathrm{ray}_{\partial\Omega}(x) = p_{\partial\Omega}^{-1}(x)$.

We now recall some classical results (see [17], chapter 7, theorems 3.1, 3.3 and [6]).

Lemma 3.4. Let $\Omega \subset \mathbb{R}^d$ be a Lipschitz bounded open set.
- A point $x \notin \partial\Omega$ has a unique projection $p_{\partial\Omega}(x)$ on $\partial\Omega$ if and only if $x \notin \Sigma$. In such a case, it satisfies $d(x, \partial\Omega) = |p_{\partial\Omega}(x) - x|$ and the gradient of d_Ω at x reads

$$\nabla d_\Omega(x) = \frac{p_{\partial\Omega}(x) - x}{d_\Omega(x)}.$$

- As a consequence of Rademacher's theorem ([19], section 3.1.2), Σ has zero Lebesgue measure in $\mathbb{R}^d$. Furthermore, when Ω is $\mathcal{C}^2$, $\overline{\Sigma}$ has zero Lebesgue measure too [27].

- For any $x \in \mathbb{R}^d$, $p \in \Pi_{\partial\Omega}(x)$, $\alpha \in [0, 1]$, denoting $x_\alpha := p + \alpha(x - p)$ the points of the ray of x lying between p and x, we have $d_\Omega(x_\alpha) = \alpha d_\Omega(x)$ and $\Pi_{\partial\Omega}(x_\alpha) \subset \Pi_{\partial\Omega}(x)$.
- If Ω is of class $\mathcal{C}^k$, for $k \geq 2$, then d_Ω is $\mathcal{C}^k$ too in a tubular neighborhood of $\partial\Omega$. In that case, d_Ω is differentiable at every point $x \in \partial\Omega$, and $\nabla d_\Omega(x) = n(x)$, the unit normal vector to Ω.

Unfortunately, the signed distance function is not, strictly speaking, shape differentiable in the sense of Definition 2.1. One reason is the lack of smoothness of the gradient of d_Ω at the skeleton Σ. However, its pointwise values $d_\Omega(x)$ are shape differentiable for $x \in D \setminus \Sigma$. This is the purpose of the next result which can be found in [18] (without much details however ; see [14] for detailed and complete proofs).

Proposition 3.5. Assume $\Omega \subset D$ is an open set of class $\mathcal{C}^1$, and fix a point $x \notin \Sigma$. Then $\theta \mapsto d_{(Id+\theta)\Omega}(x)$ is Gâteaux-differentiable at $\theta = 0$, as an application from $W^{1,\infty}(D, \mathbb{R}^d)$ into $\mathbb{R}$, and its derivative is

$$d'_\Omega(\theta)(x) = -\theta(p_{\partial\Omega}(x)) \cdot n(p_{\partial\Omega}(x)).$$

Remark 3.6. Actually, a more general result than that of Proposition 3.5 holds. Indeed, retaining the hypothesis that Ω is of class $\mathcal{C}^1$, for any point $x \in \mathbb{R}^d$, and denoting, for a real parameter $t > 0$,

$$\Omega_{t\theta} = (I + t\theta)\Omega,$$

the application $t \mapsto d_{\Omega_{t\theta}}(x)$ is *right-differentiable* at $t = 0^+$, and

- if $x \in \Omega$, $\frac{d}{dt}\left(d_{\Omega_{t\theta}}(x)\right)|_{t=0^+} = -\inf_{y \in \Pi_{\partial\Omega}(x)} \theta(y) \cdot n(y)$.
- if $x \in {}^c\overline{\Omega}$, $\frac{d}{dt}\left(d_{\Omega_{t\theta}}(x)\right)|_{t=0^+} = -\sup_{y \in \Pi_{\partial\Omega}(x)} \theta(y) \cdot n(y)$.

Of course, these formulae agree with the previous result since $\Pi_{\partial\Omega}(x) = \{p_{\partial\Omega}(x)\}$ if $x \notin \Sigma$.

Note also that a similar analysis could be performed when Ω is only assumed to be Lipschitz. However, the results are then more tedious to write, since the normal vector field n is not defined everywhere on $\partial\Omega$ (which is an indicator of specific geometric phenomena, see [14]).

Remark 3.7. The signed distance function can also be seen as a solution of the following Hamilton-Jacobi equation

$$\begin{cases} |\nabla d_\Omega(x)| = 1 & \text{in } D, \\ d_\Omega(x) = 0 & \text{on } \partial\Omega. \end{cases}$$

The behavior of the variations of d_Ω with respect to the domain can be retrieved by a formal computation. Indeed, assuming that d_Ω is shape differentiable, a formal computation yields that the directional shape derivative $d'_\Omega(\theta)$ satisfies

$$\begin{cases} \nabla d_\Omega(x) \cdot d'_\Omega(\theta)(x) = 0 & \text{in } D, \\ d'_\Omega(\theta)(x) = -\theta(x) \cdot n(x) & \text{on } \partial\Omega. \end{cases}$$

Corollary 3.8. Let Ω be a bounded domain of class $\mathcal{C}^1$ and $m(x, s) : \mathbb{R}^d_x \times \mathbb{R}_s \to \mathbb{R}$ a function of class $\mathcal{C}^1$. Define the functional $J(\Omega)$ as

$$(18) \qquad\qquad J(\Omega) = \int_D m(x, d_\Omega(x)) \, dx.$$

The application $\theta \mapsto J((Id + \theta)\Omega)$, from $W^{1,\infty}(D, \mathbb{R}^d)$ into $\mathbb{R}$, is Gâteaux-differentiable at $\theta = 0$ and its derivative reads

$$(19) \qquad\qquad J'(\Omega)(\theta) = -\int_D \frac{\partial m}{\partial s}(x, d_\Omega(x)) \, \theta(p_{\partial\Omega}(x)) \cdot n(p_{\partial\Omega}(x)) \, dx.$$

The shape derivative (19) satisfies the Hadamard structure theorem since it depends only on the values of $\theta \cdot n$ on the boundary of $\partial\Omega$. However (19) is not a surface integral on $\partial\Omega$ as usual. Therefore the task of the next subsection is to transform (19) into a surface integral by using the notion of *rays* (see Definition 3.3), along which d_Ω and $p_{\partial\Omega}$ take very simple forms, altogether with the coarea formula.
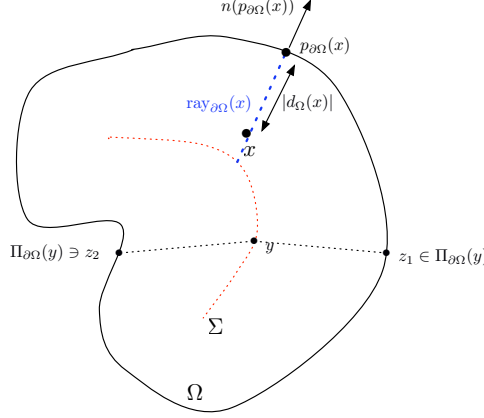
FIGURE 3. For a point x lying outside the skeleton Σ of Ω, unique projection point $p_{\partial\Omega}(x)$ and line segment $\mathrm{ray}_{\partial\Omega}(x)$. For a point $y \in \Sigma$, at least two points z_1, z_2 belong to the set of projections $\Pi_{\partial\Omega}(y)$.

3.3. **An application of the coarea formula to integral functions of the signed distance function.**

The purpose of this section is to derive a Fubini-like formula for integrals of the form (19) and transform them in surface integrals. To this end, we use the following coarea formula [12].

Proposition 3.9. Let X, Y be two smooth Riemannian manifolds of respective dimension $m \geq n$, and $f : X \to Y$ a surjective map of class $\mathcal{C}^1$, whose differential $\nabla f(x) : T_x X \to T_{f(x)} Y$ is surjective for almost every $x \in X$. Let φ an integrable function over X. Then:

$$\int_X \varphi(x)dx = \int_Y \left(\int_{z \in f^{-1}(y)} \varphi(z) \frac{1}{\mathrm{Jac}(f)(z)} dz \right) dy$$

where $\mathrm{Jac}(f)(z)$ is the the Jacobian of the function f.

Remark 3.10. If $m \geq n$, and $f : \mathbb{R}^m \to \mathbb{R}^n$ is a differentiable function at a point $x \in \mathbb{R}^m$, the Jacobian $\mathrm{Jac}(f)(x)$ of f at x is defined as

$$\mathrm{Jac}(f)(x) := \sqrt{\det(\nabla f(x) \, \nabla f(x)^T)}.$$

The definition of the Jacobian is similar when f is a map between two Riemannian manifolds X and Y, once the tangent planes $T_x X, T_{f(x)} Y$ have been identified to $\mathbb{R}^m$ and $\mathbb{R}^n$ respectively (see [12], exercise $III.11$). In any case, the Jacobian is positive $\mathrm{Jac}(f)(x) > 0$ if and only if $\nabla f(x)$ is of maximum rank, or equivalently $\nabla f(x)$ is surjective from $\mathbb{R}^m$ to $\mathbb{R}^n$.

We apply this formula in our context to $X = \Omega$, $Y = \partial\Omega$ and $f = p_{\partial\Omega}$. To apply Proposition 3.9 we need the differentiability of $p_{\partial\Omega}$ which will be deduced from the following classical result on the second-order differentiability of the signed distance function [10].

Lemma 3.11. Assume Ω is of class $\mathcal{C}^2$. For $i = 1, ..., d-1$, denote by κ_i the principal curvatures of $\partial\Omega$ and e_i its associated directions (see Figure 4). For every $x \in D$, and every $y \in \Pi_{\partial\Omega}(x)$, we have

(20) $$-\kappa_i(y)d_\Omega(x) \leq 1, \quad 1 \leq i \leq d-1.$$

Define Γ the singular set of Ω, namely the set of points $x \notin \Sigma$ such that, for some i, one of the inequality (20) is actually an equality. Then, $\overline{\Sigma} = \Sigma \cup \Gamma$ and $\overline{\Sigma}$ has zero Lebesgue measure. If $x \notin \overline{\Sigma}$, then all inequalities (20) are strict and d_Ω is twice differentiable at x. Its Hessian reads

$$\mathcal{H}d_\Omega(x) = \sum_{i=1}^{d-1} \frac{\kappa_i(p_{\partial\Omega}(x))}{1 + \kappa_i(p_{\partial\Omega}(x))d_\Omega(x)} e_i(p_{\partial\Omega}(x)) \otimes e_i(p_{\partial\Omega}(x)).$$

11

Lemma 3.12. Let $x \in D \setminus \overline{\Sigma}$. The projection map $p_{\partial\Omega}$ is differentiable at x and, in the orthonormal basis $\{e_1, ..., e_{d-1}, n\} (p_{\partial\Omega}(x))$ of $\mathbb{R}^d$ (see Figure 4), its gradient is a $d \times d$ diagonal matrix

(21)
$$\nabla p_{\partial\Omega}(x) = \begin{pmatrix} 1 - \frac{d_\Omega(x)\kappa_1}{1+d_\Omega(x)\kappa_1} & 0 & \cdots & 0 \\ 0 & \ddots & \ddots & \vdots \\ \vdots & \ddots & 1 - \frac{d_\Omega(x)\kappa_{d-1}}{1+d_\Omega(x)\kappa_{d-1}} & 0 \\ 0 & \cdots & 0 & 0 \end{pmatrix},$$

where the the principal curvatures κ_i are evaluated at $p_{\partial\Omega}(x)$.

Proof. The proof starts from the characterization of the projection map when $x \in D \setminus \Sigma$ (see Lemma 3.4)

$$p_{\partial\Omega}(x) = x - d_\Omega(x)\nabla d_\Omega(x).$$

This last equality can then be differentiated once more for $x \in D \setminus \overline{\Sigma}$

(22)
$$\nabla p_{\partial\Omega}(x) = Id - \nabla d_\Omega(x) \, \nabla d_\Omega(x)^T - d_\Omega(x)\mathcal{H}d_\Omega(x).$$

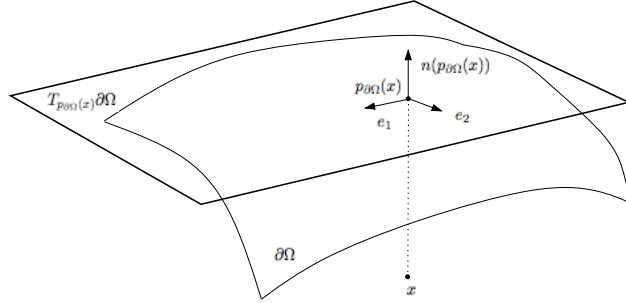Since $\nabla d_\Omega(x) = n(p_{\partial\Omega}(x))$, a simple calculation ends the proof. $\qquad \square$

FIGURE 4. Principal directions, normal vector at the projection point of $x \in \mathbb{R}^d$.

We now come to the main result of this section.

Corollary 3.13. Let $\Omega \subset D$ be a $\mathcal{C}^2$ bounded domain, and let φ an integrable function over D. Then,

(23)
$$\int_D \varphi(x)dx = \int_{\partial\Omega} \left(\int_{\text{ray}_{\partial\Omega}(y) \cap D} \varphi(z) \prod_{i=1}^{d-1} (1 + d_\Omega(z)\kappa_i(y))dz \right) dy,$$

where z denotes a point in the ray emerging from $y \in \partial\Omega$ and dz is the line integration along that ray.

Proof. Since $\overline{\Sigma}$ is of zero Lebesgue measure, we have

$$\int_D \varphi(x)dx = \int_{D\setminus\overline{\Sigma}} \varphi(x)dx.$$

Applying Lemmas 3.11 and 3.12, $p_{\partial\Omega}$ is a surjective and differentiable map from $D \setminus \overline{\Sigma}$ into $\partial\Omega$, with a positive finite Jacobian for any $x \in D \setminus \overline{\Sigma}$

$$\text{Jac}\,(p_{\partial\Omega})\,(x) = \frac{1}{\displaystyle\prod_{i=1}^{d-1}\left(1 + d_\Omega(x)\kappa_i(p_{\partial\Omega}(x))\right)}.$$

Proposition 3.9 then yields the desired result. $\qquad \square$

3.4. **Shape derivative of the compliance in the multi-materials setting.**

We now have all the necessary ingredients to differentiate the cost function (2) with respect to the domain. We keep the geometrical assumptions of section 2, namely for a given bounded open set $D \subset \mathbb{R}^d$ which is partitioned in two subdomains $\Omega^0, \Omega^1 \subset D$, Ω^0 is a strict subset of D in the sense that its boundary Γ, as well as its thick approximation, does not touch ∂D (see Figure 1) and Γ is smooth.

We define the adjoint problem

$$
(24) \qquad \begin{cases} -\mathrm{div}\left(A_{\Omega^0,\varepsilon}\, e(p)\right) & = & -j'(x,u) & \text{in } D, \\ p & = & 0 & \text{on } \Gamma_D, \\ (A_1\, e(p))\cdot n & = & -k'(x,u) & \text{on } \Gamma_N, \end{cases}
$$

where the symbol $\prime$ denotes differentation with respect to u.

Our main result is the following.

Theorem 3.14. The objective function (2) is shape differentiable in the sense of Gâteaux, namely $\theta \mapsto J((Id + \theta)\Omega^0)$ admits a Gâteaux derivative at $\theta = 0$, which is

$$
(25) \qquad J'(\Omega^0)(\theta) = -\int_\Gamma \theta(x)\cdot n(x)\Big(f_0(x) + f_1(x)\Big)dx, \quad \forall\, \theta \in W^{1,\infty}(D,\mathbb{R}^d),
$$

where n is the outer unit normal to Ω^0 and f_0, f_1 are scalar functions defined by

$$
f_0(x) = \int_{\mathrm{ray}_\Gamma(x)\cap\Omega^0} h'_\varepsilon\left(d_{\Omega^0}(z)\right)(A_1 - A_0)e(u)(z) : e(p)(z) \prod_{i=1}^{d-1}(1 + d_{\Omega^0}(z)\kappa_i(x))dz,
$$

$$
f_1(x) = \int_{\mathrm{ray}_\Gamma(x)\cap\Omega^1} h'_\varepsilon\left(d_{\Omega^0}(z)\right)(A_1 - A_0)e(u)(z) : e(p)(z) \prod_{i=1}^{d-1}(1 + d_{\Omega^0}(z)\kappa_i(x))dz,
$$

where z denotes a point in the ray emerging from $x \in \Gamma$.

Proof. The rigorous proof of existence of the shape derivative stems from classical arguments (typically the implicit function theorem) similar to those invoked in [32] or chapter 5 in [23]. We rather focus on the actual computation of the shape derivative and use once again the formal Lagrangian method of Céa [11]. As the computation unfolds very similarly to that in the proof of Theorem 3.6 in [4], we limit ourselves to the main arguments.

Define first the functional space $V := \{v \in H^1(D)^d \text{ such that } v = 0 \text{ on } \Gamma_D\}$, in which are sought the solution of the state equation (17) and of the adjoint equation (24). We introduce the Lagrangian $\mathcal{L} : W^{1,\infty}\left(D,\mathbb{R}^d\right) \times V \times V \to \mathbb{R}$, defined by

$$
(26) \quad \mathcal{L}(\theta,v,q) = \int_D j(x,v)\,dx + \int_{\Gamma_N} k(x,v)\,ds + \int_D A_{(Id+\theta)\Omega^0,\varepsilon}e(v) : e(q)\,dx - \int_D f\cdot q\,dx - \int_{\Gamma_N} g\cdot q\,ds.
$$

Here, q is intended as the Lagrange multiplier associated to the enforcement of the state equation. As usual, stationarity of the Lagrangian provides the optimality conditions for the minimization problem. At $\theta = 0$, cancelling the partial derivative of $\mathcal{L}$ with respect to q yields the variational formulation of the state u. In the same way, the nullity of the partial derivative of $\mathcal{L}$ with respect to v leads to the variational formulation of the adjoint p.

Eventually, the shape derivative of the objective function is the partial derivative of $\mathcal{L}$ with respect to θ, evaluated at u and p

$$
J'(\Omega^0)(\theta) = \frac{\partial\mathcal{L}}{\partial\theta}(0,u,p)(\theta).
$$

Some elementary algebra, using the shape differentiability of $d_{\Omega^0}(x)$ for almost every $x \in D$, yields

$$
(27) \qquad \begin{aligned} J'(\Omega^0)(\theta) & = & \int_D \left(A_{(Id+\theta)\Omega^0,\varepsilon}\right)'(\theta)\,e(u) : e(p)\,dx \\ & = & -\int_D h'_\varepsilon(d_{\Omega^0}(x))\,(\theta(p_\Gamma(x))\cdot n(p_\Gamma(x)))\,(A_1 - A_0)e(u) : e(p)\,dx, \end{aligned}
$$

where $\left(A_{(Id+\theta)\Omega^0,\varepsilon}\right)'(\theta)$ is the directional shape derivative of $A_{(Id+\theta)\Omega^0,\varepsilon}$ while h'_ε is the standard derivative of the real function h_ε. It remains to transform this expression by the coarea formula in order to deduce a boundary integral. Using formula (23) for (27), we get

$$J'(\Omega^0)(\theta) = -\int_\Gamma \theta(x) \cdot n(x) \left(\int_{\mathrm{ray}_\Gamma(x)\cap D} h'_\varepsilon(d_{\Omega^0}(z))(A_1 - A_0)e(u)(z) : e(p)(z) \prod_{i=1}^{d-1} (1 + d_{\Omega^0}(z)\kappa_i(x))dz \right) dx.$$

Now decomposing the above integral over Ω^0 and Ω^1 readily yields the desired result. $\qquad\square$

Remark 3.15. Theorem 3.14 provides a simple way of choosing a descent direction for a shape gradient based algorithm. Indeed it is enough to perturb the interface Γ by choosing the vector field

$$\theta(x) = \Big(f_0(x) + f_1(x)\Big)n(x),$$

which ensures that the directional derivative (25) is negative and thus yields a decrease of the objective function (3). This is in sharp contrast with Corollary 3.8 which provided formula (19) for the shape derivative. However it was impossible to extract directly from (19) an explicit value of θ which was a guaranteed descent direction.

Remark 3.16. In the case of compliance minimization, namely for the objective function (3), we have $j' = f$, $k' = g$ and thus $p = -u$. If we assume that material 1 is stronger than material 0, in the sense that $A^1 \geq A^0$ as positive definite tensors, we deduce from the formulas of Theorem 3.14 that both f_0 and f_1 are non-positive because $1 + \kappa_i(x)d_{\Omega^0}(z) \geq 0$ by virtue of Lemma 3.11. Thus, a descent direction is obtained by choosing θ such that $\theta(x) \cdot n(x) < 0$ on Γ, namely we expend Ω^1. This is in accordance with the mechanical intuition that a more robust mixture of the two materials is achieved when A^1 prevails over A^0. Of course, for the problem to be reasonable, a volume constraint is imposed on the phases.

3.5. **Approximate formulas for the shape derivative.**

Although formula (25) is satisfying from a mathematical point of view, its numerical evaluation is not completely straightforward. There are two delicate issues. First, one has to compute the principal curvatures $\kappa_i(x)$ for any point $x \in \Gamma$ on the interface. Second, one has to perform a 1-d integration along the rays of the energy-like quantity $[A]e(u) : e(p)$. This is a classical task in the level-set framework [39] but, still, it is of interest to devise a simpler approximate formula for the shape derivative.

A first approximate formula is to assume that the interface is roughly plane, namely to assume that the principal curvatures κ_i vanish. In such a case we obtain a "Jacobian-free" approximate shape derivative

$$(28)\qquad \begin{aligned} J'(\Omega^0)(\theta) &= -\int_\Gamma \theta(x) \cdot n(x)\Big(f_0(x) + f_1(x)\Big)dx \\ f_i(x) &= \int_{\mathrm{ray}_\Gamma(x)\cap\Omega^i} h'_\varepsilon(d_{\Omega^0}(z))(A_1 - A_0)e(u)(z) : e(p)(z)dz. \end{aligned}$$

A second approximate formula is obtained when the smoothing parameter ε is small. Note that, since the support of the function h'_ε is of size 2ε, the integral in formula (25) is confined to a tubular neighborhood of Γ of width 2ε. Therefore, if ε is small, one may assume that the functions depending on z are constant along each ray, equal to their value at $x \in \Gamma$. In other words, for small ε we assume

$$e(u)(z) \approx e(u)(x), \quad e(p)(z) \approx e(p)(x) \text{ and } d_{\Omega^0}(z) \approx d_{\Omega^0}(x) = 0,$$

which yields the approximate formulas, for $x \in \Gamma$,

$$f_0(x) \approx (A_1 - A_0)e(u)(x) : e(p)(x) \int_{ray_\Gamma(x)\cap\Omega^0} h'_\varepsilon(d_{\Omega^0}(z))\ dz,$$

$$f_1(x) \approx (A_1 - A_0)e(u)(x) : e(p)(x) \int_{ray_\Gamma(x)\cap\Omega^1} h'_\varepsilon(d_{\Omega^0}(z))\ dz.$$

Furthermore, most rays have a length larger than 2ε so that

$$\int_{ray_\Gamma(x)\cap\Omega^0} h'_\varepsilon(d_{\Omega^0}(z))\ dz + \int_{ray_\Gamma(x)\cap\Omega^1} h'_\varepsilon(d_{\Omega^0}(z))\ dz = h_\varepsilon(\varepsilon) - h_\varepsilon(-\varepsilon) = 1.$$

14

In turn we obtain the following approximate formula for (25)

$$(29) \qquad J'(\Omega^0)(\theta) \approx -\int_\Gamma (A_1 - A_0)e(u) : e(p)\, \theta \cdot n\, dx,$$

which is nothing but the discrete shape derivative (13) that we obtained in the sharp-interface case. This computation seems a bit miraculous but makes sense as a kind of commutation property between interface regularization and optimization.

Our numerical results show that the latter simplification (29), which we shall refer to as the *approximate shape derivative*, works very well in practice for problems of compliance minimization. Formula (29) is also used by other authors in their numerical simulations [50].

3.6. Convergence of the smoothed-interface shape optimization problem to the sharp-interface problem.

When the smoothed-interface setting is used as an approximation of the sharp-interface case, it is a natural task to prove that this approximation is mathematically consistent. In this section, we present a result in this direction. More specifically, for a given regular interface Γ, we prove that the shape gradient obtained in Theorem 3.14 for a smoothed transition layer of width 2ε converges, as ε goes to 0, to the corresponding shape gradient in the sharp-interface context, recalled in Proposition 2.2.

To set ideas, let us limit ourselves to the case of compliance minimization, the case of a general objective function such as (2) being no different in principle. In order to make explicit the dependence on the half-thickness ε of the smoothed transmission area, the solution of the state system (17) is denoted u_ε in this section. Similarly the stress tensor is $\sigma(u_\varepsilon) = A_{\Omega^0,\varepsilon}\, e(u_\varepsilon)$ and the compliance is

$$J_\varepsilon(\Omega^0) = \int_D \sigma(u_\varepsilon) : e(u_\varepsilon)\, dx.$$

The solution of the state system (1) in the sharp-interface case is still denoted as u, and the associated compliance as $J(\Omega^0)$.

To find the limit of $J'_\varepsilon(\Omega_0)$, as $\varepsilon \to 0$, requires some knowledge of the asymptotic behavior of $e(u_\varepsilon)$ and $\sigma(u_\varepsilon)$ in the vicinity of the interface Γ. Unfortunately, one cannot expect all the components of $e(u_\varepsilon)$ and $\sigma(u_\varepsilon)$ to converge toward their counterpart in $e(u)$ and $\sigma(u)$ in any space of smooth enough functions. Indeed, for fixed ε, $e(u_\varepsilon)$ is smooth over D (because so is the associated Hooke's tensor), whereas we recalled in Remark 2.3 that $e(u)_{\tau n}$ and $e(u)_{nn}$ are discontinuous across Γ, as imposed by the transmission conditions. However, some of the components of $e(u_\varepsilon)$ and $\sigma(u_\varepsilon)$ do behave well as $\varepsilon \to 0$. This is the purpose of the following lemma, which is a consequence of rather classical results in elliptic regularity theory (see [14] for a proof).

Lemma 3.17. Assuming Γ is a $\mathcal{C}^2$ interface, there exists a tubular neighborhood $V \subset\subset D$ of Γ such that one can define a smooth extension in V of the normal n and of a set of tangentials and orthonormal vectors τ. Then, the following strong convergences hold true

$$\begin{aligned}
e(u_\varepsilon)_{\tau\tau} &\xrightarrow{\varepsilon\to 0} e(u)_{\tau\tau} &&\text{in } H^1(V)^{(d-1)^2} \text{ strong,} \\
\sigma(u_\varepsilon)_{\tau n} &\xrightarrow{\varepsilon\to 0} \sigma(u)_{\tau n} &&\text{in } H^1(V)^d \text{ strong,} \\
\sigma(u_\varepsilon)_{nn} &\xrightarrow{\varepsilon\to 0} \sigma(u)_{nn} &&\text{in } H^1(V) \text{ strong.}
\end{aligned}$$

Remark 3.18. The components of the strain and stress tensors which converge in Lemma 3.17 correspond exactly to those which are continuous through the interface Γ as explained in Remark 2.3.

We are now in a position to state the main result of the present section which implies that the shape derivative of the smoothed-interface objective function is a consistent approximation of the corresponding shape derivative in the sharp-interface case.

Theorem 3.19. Under the above assumptions, we have

$$\lim_{\varepsilon\to 0} J'_\varepsilon(\Omega^0)(\theta) = J'(\Omega^0)(\theta) \quad \forall \theta \in W^{1,\infty}(D, \mathbb{R}^d).$$

15

Sketch of the proof. As the proof involves rather classical arguments, but tedious computations, we limit ourselves with an outline of the main steps, referring to [14] for details. The goal is to pass to the limit $\varepsilon \to 0$ in formula (25), for a fixed $\theta \in W^{1,\infty}(D, \mathbb{R}^d)$. To achieve this, the rays $\mathrm{ray}_\Gamma(x) \cap \Omega^0$ and $\mathrm{ray}_\Gamma(x) \cap \Omega^1$ are expressed as integrals over the segment $(0,1)$. Therefore, (25) becomes

$$J'_\varepsilon(\Omega^0)(\theta) = -\int_\Gamma \theta(x) \cdot n(x) \Big(f_0^\varepsilon(x) + f_1^\varepsilon(x) \Big) dx,$$

where $f_0^\varepsilon, f_1^\varepsilon \in L^1(\Gamma)$ are defined as

(30)
$$f_0^\varepsilon(x) = \int_{-1}^0 h'_\varepsilon(s\varepsilon)(A_1 - A_0)e(u_\varepsilon)(x + s\varepsilon n(x)) : e(u_\varepsilon)(x + s\varepsilon n(x)) \, k_\varepsilon(x, s) \, ds,$$

(31)
$$f_1^\varepsilon(x) = \int_0^1 h'_\varepsilon(s\varepsilon)(A_1 - A_0)e(u_\varepsilon)(x + s\varepsilon n(x)) : e(u_\varepsilon)(x + s\varepsilon n(x)) \, k_\varepsilon(x, s) \, ds,$$

with

$$k_\varepsilon(x, s) = \prod_{i=1}^{d-1} (1 + s\varepsilon\kappa_i(x)).$$

Since $h'_\varepsilon(s\varepsilon)$ does not depend on ε, to pass to the limit in (30) and (31) requires merely the following simple technical convergence result (see [14] for a proof)

(32)
$$\int_0^1 v(s) \, f_\varepsilon(x + s\varepsilon n(x))g_\varepsilon(x + s\varepsilon n(x)) \, ds \xrightarrow{\varepsilon \to 0} \left(\int_0^1 v(s) \, ds \right) f(x)g(x) \quad \text{in } L^1(\Gamma)$$

for a smooth function $v(s)$ and any sequences $f_\varepsilon, g_\varepsilon \in H^1(D)$, which converge strongly in $H^1(D)$ to f, g respectively. In order to apply (32) we rewrite expressions (30) and (31) in terms of the components $e(u_\varepsilon)_{\tau\tau}$ and $\sigma(u_\varepsilon)_{\tau n}$, $\sigma(u_\varepsilon)_{nn}$ of the strain and stress tensors, which have a fine behavior at the limit $\varepsilon \to 0$ as guaranteed by Lemma 3.17. After some algebra, we obtain the following rearrangement for the integrand in f_0^ε and f_1^ε:

$$
\begin{aligned}
(A_1 - A_0)e(u_\varepsilon) : e(u_\varepsilon)(x + s\varepsilon n(x)) = \quad & \mu'(s) \, (e(u_\varepsilon)_{\tau\tau} : e(u_\varepsilon)_{\tau\tau}) \, (x + s\varepsilon n(x)) \\
+ \quad & \frac{\mu'(s)}{\mu(s)^2} \, (\sigma^\varepsilon(u_\varepsilon)_{\tau n} \cdot \sigma^\varepsilon(u_\varepsilon)_{\tau n}) \, (x + s\varepsilon n(x)) \\
+ \quad & \frac{4\mu^2(s)\lambda'(s) + 2\mu'(s)\lambda^2(s)}{(2\mu(s) + \lambda(s))^2} \, \mathrm{tr}(e(u_\varepsilon)_{\tau\tau})^2(x + s\varepsilon n(x)) \\
+ \quad & \frac{2\mu'(s) + \lambda'(s)}{(2\mu(s) + \lambda(s))^2} \, \sigma^\varepsilon(u_\varepsilon)_{nn}^2(x + s\varepsilon n(x)) \\
+ \quad & \frac{4\mu(s)\lambda'(s) - 4\mu'(s)\lambda(s)}{(2\mu(s) + \lambda(s))^2} \, (\sigma^\varepsilon(u_\varepsilon)_{nn} \, \mathrm{tr}(e(u_\varepsilon)_{\tau\tau})) \, (x + s\varepsilon n(x))
\end{aligned}
$$

with

$$\lambda(s) = \lambda_0 + h_\varepsilon(s\varepsilon)(\lambda_1 - \lambda_0), \quad \mu(s) = \mu_0 + h_\varepsilon(s\varepsilon)(\mu_1 - \mu_0),$$

where λ_0, μ_0 and λ_1, μ_1 are the Lamé coefficients of materials 0, 1 respectively. Note that all the functions of s involving $\lambda(s)$ and $\mu(s)$ appearing in the above expression arise as exact derivatives of functions of $\lambda(s)$ and $\mu(s)$. Passing to the limit in the above expression using (32) leads to

$$(f_0^\varepsilon + f_1^\varepsilon) \to \mathcal{D}(u, u) \quad \text{in } L^1(\Gamma),$$

where $\mathcal{D}(u, u)$ is defined as

$$
\begin{aligned}
\mathcal{D}(u, u)(x) = \quad & 2 \, [\mu] \, e(u)_{\tau\tau}(x) : e(u)_{\tau\tau}(x) - \left[\tfrac{1}{\mu}\right] \sigma(u)_{\tau n}(x) \cdot \sigma(u)_{\tau n}(x) \\
+ \quad & \left[\tfrac{2\lambda\mu}{(2\mu+\lambda)}\right] \mathrm{tr}(e(u)_{\tau\tau}(x))^2 - \left[\tfrac{1}{2\mu+\lambda}\right] \sigma(u)(x)_{nn}^2 \\
+ \quad & \left[\tfrac{2\lambda}{2\mu+\lambda}\right] \sigma(u)_{nn}(x) \, \mathrm{tr}(e(u)_{\tau\tau}(x))
\end{aligned}
$$

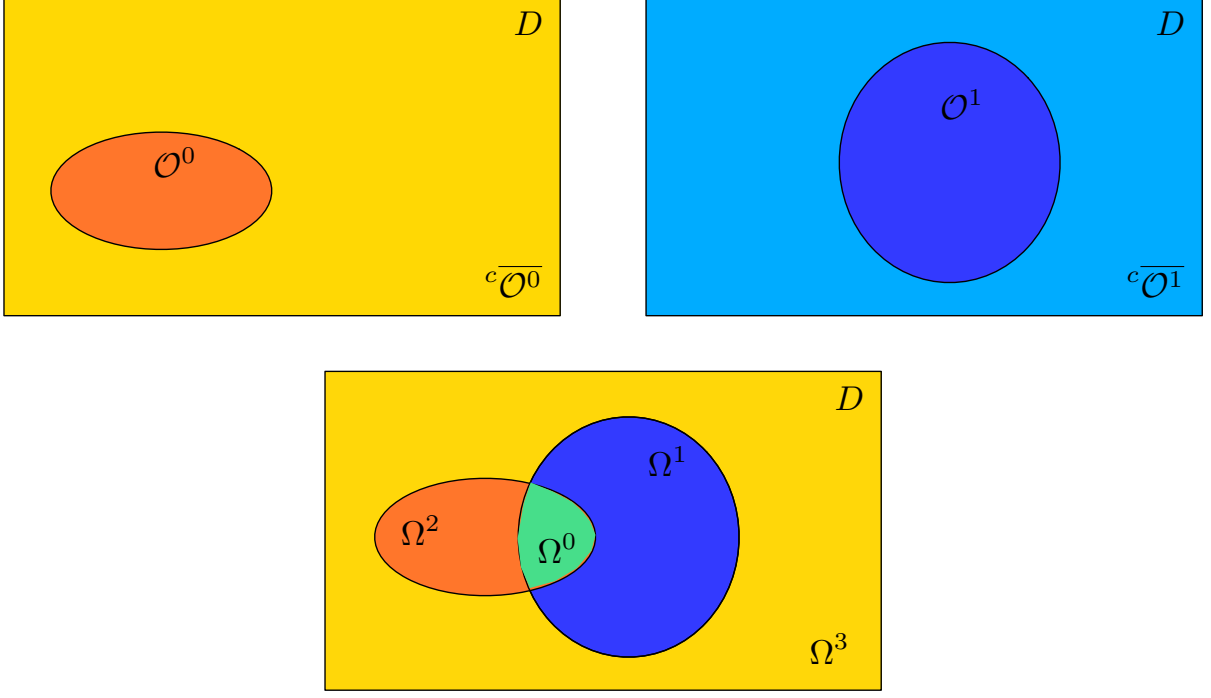which after some algebra rewrites as (5). This completes the proof. $\qquad\square$

FIGURE 5. Two subdomains of D (top) and the four phase domains derived by combining them together (down).

4. EXTENSION TO MORE THAN 2 MATERIALS

The methods presented in sections 2 and 3 for two phases can be extended to the case of several materials to be optimally placed in the domain D, following a classical idea in the level-set framework [48], [50].

Hitherto, we considered a single subdomain $\Omega^0 \subset D$, which allows to account for two separate phases within D, occupying respectively the domains Ω^0 and $\Omega^1 := {}^c\overline{\Omega^0}$ (where ^{c} denotes the complementary part in D). To consider more phases, we introduce m subdomains $\mathcal{O}^0, ..., \mathcal{O}^{m-1} \subset D$ which are not subject to any geometrical constraints (they can intesect, or not, and they don't need to cover D). These m subdomains allows us to treat up to 2^m distinct phases, filling respectively the phase domains $\Omega^0, ..., \Omega^{2^m-1} \subset D$, defined as (see Figure 4)

$$(33) \quad \begin{cases} \Omega^0 & = & \mathcal{O}^0 \cap \mathcal{O}^1 \cap ... \cap \mathcal{O}^{m-1}, \\ \Omega^1 & = & {}^c\overline{\mathcal{O}^0} \cap \mathcal{O}^1 \cap ... \cap \mathcal{O}^{m-1}, \\ & \vdots & \\ \Omega^{2^m-1} & = & {}^c\overline{\mathcal{O}^0} \cap {}^c\overline{\mathcal{O}^1} \cap ... \cap {}^c\overline{\mathcal{O}^{m-1}}. \end{cases}$$

Note that $\Omega^0, ..., \Omega^{2^m-1}$ is a partition of D. To simplify the exposition, from now on we take $m = 2$, meaning that we consider four different materials, with respective Hooke's law A_0, A_1, A_2, A_3. Two subdomains $\mathcal{O}^0, \mathcal{O}^1$ of D are then introduced, and each material A_i fills an area $\Omega^i \subset D$, defined through formula (33).

For the sharp-interface problem, the definition of the mixture Hooke's tensor A_χ is standard. Introducing χ_0 and χ_1 the characteristic functions of $\mathcal{O}^0$ and $\mathcal{O}^1$, respectively, we define

$$(34) \quad A_\chi(x) := \chi_0(x)\chi_1(x)A_0 + (1 - \chi_0(x))\,\chi_1(x)A_1 + \chi_0(x)\,(1 - \chi_1(x))\,A_2 + (1 - \chi_0(x))\,(1 - \chi_1(x))\,A_3.$$

For the smoothed-interface problem, we propose a formula inspired from (34)

$$(35) \quad \begin{aligned} A_{\mathcal{O}^0,\mathcal{O}^1,\varepsilon}(x) & = & (1 - h_\varepsilon(d_{\mathcal{O}^0}(x)))(1 - h_\varepsilon(d_{\mathcal{O}^1}(x)))A_0 + h_\varepsilon(d_{\mathcal{O}^0}(x))(1 - h_\varepsilon(d_{\mathcal{O}^1}(x)))A_1 \\ & + & (1 - h_\varepsilon(d_{\mathcal{O}^0}(x)))h_\varepsilon(d_{\mathcal{O}^1}(x))A_2 + h_\varepsilon(d_{\mathcal{O}^0}(x))h_\varepsilon(d_{\mathcal{O}^1}(x))A_3, \end{aligned}$$

17

where h_ε is the smooth approximation (16) of the Heaviside function and $d_{\mathcal{O}^0}, d_{\mathcal{O}^1}$ are the signed distance functions to $\mathcal{O}^0$ and $\mathcal{O}^1$ respectively. Of course, there are other interpolation formulas and any alternative choice which, as (35), satisfies the following consistency

$$
(36) \qquad A_{\mathcal{O}^0,\mathcal{O}^1,\varepsilon}(x) = \begin{cases}
A_0 & \text{if} \quad d_{\mathcal{O}^0}(x) < -\varepsilon \quad \text{and} \quad d_{\mathcal{O}^1}(x) < -\varepsilon, \\
A_1 & \text{if} \quad d_{\mathcal{O}^0}(x) > +\varepsilon \quad \text{and} \quad d_{\mathcal{O}^1}(x) < -\varepsilon, \\
A_2 & \text{if} \quad d_{\mathcal{O}^0}(x) < -\varepsilon \quad \text{and} \quad d_{\mathcal{O}^1}(x) > +\varepsilon, \\
A_3 & \text{if} \quad d_{\mathcal{O}^0}(x) > +\varepsilon \quad \text{and} \quad d_{\mathcal{O}^1}(x) > +\varepsilon, \\
\text{a smooth interpolation between } A_0, A_1, A_2, A_3 \text{ otherwise,}
\end{cases}
$$

will do. In particular, for applications in material science where the thick interface has a clear physical interpretation, one could choose a physically relevant choice of the interpolant Hooke's law for the mixture of A_0, A_1, A_2, A_3 in the intermediate areas, like a sequential laminate or another microstructure achieving Hashin and Shtrikman bounds [31]. On the other hand, if the smoothed-interface problem is merely a mathematical approximation of the sharp-interface case, then it is a consistent approximation since, as the regularizing parameter ε goes to 0, the smooth tensor $A_{\mathcal{O}^0,\mathcal{O}^1,\varepsilon}$ converges to the discontinuous one A_χ.

In the multiphase case, the definition of the objective function (2) does not change

$$
(37) \qquad J(\mathcal{O}^0, \mathcal{O}^1) = \int_D j(x, u) \, dx + \int_{\Gamma_N} k(x, u) \, ds,
$$

and the state or adjoint equations are the same, up to changing the previous Hooke's tensor by $A_{\mathcal{O}^0,\mathcal{O}^1,\varepsilon}$. There are now two variable subdomains, $\mathcal{O}^0, \mathcal{O}^1$, as design variables for the optimization problem. Accordingly, we introduce two separate vector fields $\theta_0, \theta_1 \in W^{1,\infty}(D, \mathbb{R}^d)$ in order to vary the subdomains $\mathcal{O}^0, \mathcal{O}^1$.

According to Corollary 3.8, the partial shape derivative of the objective function (37) with respect to $\mathcal{O}^0$ and $\mathcal{O}^1$, which we shall denote as $\frac{\partial J}{\partial \mathcal{O}^0}$ and $\frac{\partial J}{\partial \mathcal{O}^1}$ respectively, in the direction of θ^0 and θ^1, respectively, are

$$
(38) \qquad \frac{\partial J}{\partial \mathcal{O}^0}(\mathcal{O}^0, \mathcal{O}^1)(\theta_0) = \int_D \theta_0(p_{\partial \mathcal{O}^0}(x)) \cdot n_0(p_{\partial \mathcal{O}^0}(x)) \frac{\partial A}{\partial d_{\mathcal{O}^0}}(d_{\mathcal{O}^0}, d_{\mathcal{O}^1}) e(u) : e(p) \, dx,
$$

$$
(39) \qquad \frac{\partial J}{\partial \mathcal{O}^1}(\mathcal{O}^0, \mathcal{O}^1)(\theta_1) = \int_D \theta_1(p_{\partial \mathcal{O}^1}(x)) \cdot n_1(p_{\partial \mathcal{O}^1}(x)) \frac{\partial A}{\partial d_{\mathcal{O}^1}}(d_{\mathcal{O}^0}, d_{\mathcal{O}^1}) e(u) : e(p) \, dx,
$$

where $A(d_{\mathcal{O}^0}, d_{\mathcal{O}^1}) = A_{\mathcal{O}^0,\mathcal{O}^1,\varepsilon}$, defined in (36). Of course, one can apply Theorem 3.14 to simplify (38) and (39) and transform them in surface integrals on $\partial \mathcal{O}^0$ and $\partial \mathcal{O}^1$.

Remark 4.1. In the sharp interface context one could compute shape derivatives of the objective function J with respect to $\mathcal{O}^0$ and $\mathcal{O}^1$ too, thus recovering formulas similar to (38) and (39). However, it is possible only if we assume that the boundary of $\mathcal{O}^0$ and $\mathcal{O}^1$ do not superpose. Indeed if, for example, $\partial \mathcal{O}^0 = \partial \mathcal{O}^1$, then moving $\mathcal{O}^0$ inside $\mathcal{O}^1$, or vice versa, implies that one phase or another one appears. This means that a topology change is occuring which cannot be handled by Hadamard method. At most, one can expect to compute two different directional derivatives (inward and outward) which clearly shows that there is no differentiability in this case. Note that there is no such difficulty in the smoothed interface setting: formulas (38) and (39) hold true for any geometrical situation of $\mathcal{O}^0$ and $\mathcal{O}^1$ since $A_{\mathcal{O}^0,\mathcal{O}^1,\varepsilon}$ is a smooth function of x in D.

5. Discussion and comparison with previous formulae in the literature

To our knowledge, the first works on multi-phase optimization using a level-set method are [29] and [50]. Further references include [30], [49], [51]. In all these works the computation of the shape derivative is not mathematically rigorous and the obtained formula are not strictly correct. Indeed, either the shape differentiation is performed in the sharp-interface case and then the non-differentiable character of the solution of (1) is ignored (as explained in section 2.2), or the shape derivative is evaluated in the smoothed-interface case and then the derivative of the signed distance function is not taken into account. Fortunately, the shape derivative formulas in [29] and [50] coincide with what we called our approximate shape derivatives obtained in Proposition 2.5 for a discretization of the sharp-interface case and in (29) for a very thin smoothed interface. A third possibility for interpreting these works is to consider that the regularization of the interface

is made with the help of the level set function ψ (used in numerical practice for representing and advecting the shape, see section 6 below) rather than with the signed distance function d_Ω. Then the differentiation is performed with respect to ψ rather than with respect to the shape Ω. It alleviates all the technical details of section 3 but it has one major flaw that we now describe.
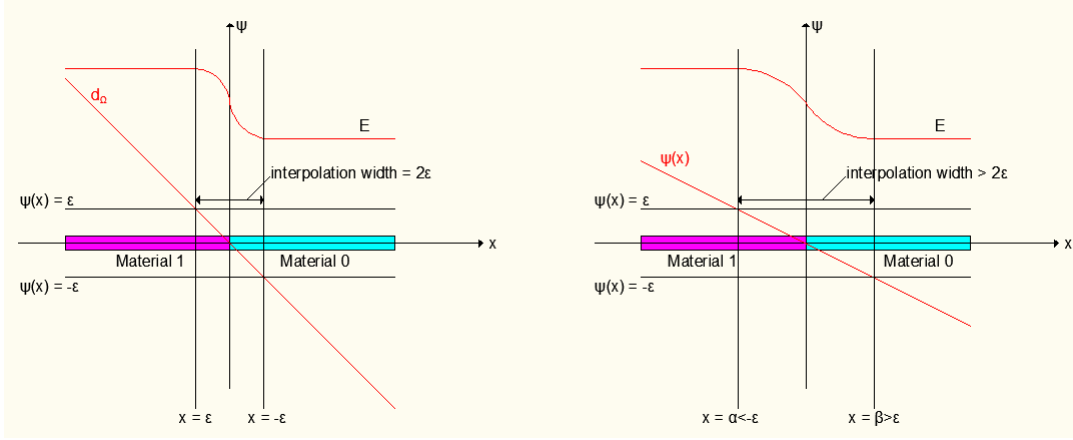

FIGURE 6. Intermediate zone for regularization with the signed distance function (left) or with a level set functions (right).

Indeed, in the context of section 3 on the smoothed interface approach, one may replace the regularization formula (15) by a similar one

$$(40) \qquad A_{\Omega^0,\varepsilon}(x) = A_0 + h_\varepsilon(\psi(x))(A_1 - A_0), \quad \forall\, x \in D,$$

where the signed distance function d_Ω has simply been replace by the level set function ψ. Then, as is done in [29] and [30], one may differentiate the objective function with respect to ψ. A serious problem that rises directly from this choice, is that the interpolation zone, where $A_{\Omega^0,\varepsilon}$ takes intermediate values between A_0 and A_1, can thicken during the optimization process, especially if the level set function ψ is not frequently reinitialized towards the signed distance function to the boundary (see Figure 6). The reason is that the interpolation zone corresponds to some kind of homogenized material made of A_0 and A_1, which is known to be more advantageous than pure phases in most problems [2]. The optimization process therefore does not only move the interface location but also flaten the level set function ψ so that the interpolation zone gets thicker. Even when the level set function is reinitialized, there remains a difficulty in the sense that the value of the objective function may change before and after reinitialization. A partial remedy to this inconvenient, as suggested in [29], is to add to the objective function a penalization term to control the enlargement.

The computation of the shape derivative is slightly different in [50]: the authors carry out the derivation with the level set function ψ but in the resulting formula they assume that ψ coincides with the signed distance function to the interface d_Ω. More precisely, following the notations of Corollary 3.8, they consider a functional

$$(41) \qquad J(\Omega) = \int_D m(x, \psi(x))\, dx,$$

where ψ is a solution of the Hamilton-Jacobi equation

$$\frac{\partial\psi}{\partial t} + \theta \cdot n\, |\nabla\psi| = 0.$$

Then, the authors claim that the shape derivative is

$$(42) \qquad J'(\Omega)(\theta) = -\int_D \frac{\partial m}{\partial \psi}(x, \psi(x))\, \theta(x) \cdot n(x)\, dx.$$

Note the difference with our formula (19), which involves the projection $p_\Gamma(x)$ of x on the boundary $\Gamma = \partial\Omega$, and that we recall as

$$J'(\Omega)(\theta) = -\int_D \frac{\partial m}{\partial \psi}(x, d_\Omega(x))\, \theta(p_\Gamma(x)) \cdot n(p_\Gamma(x))\, dx.$$

Unfortunately, there is no a priori guarantee that the transported signed distance function to the boundary $\partial\Omega$ remains the signed distance function to the transported boundary $(Id + \theta)\partial\Omega$. Therefore, the shape derivative $d'_\Omega(\theta)(x)$ cannot be replaced by the expression $\frac{\partial \psi}{\partial t} = -\theta \cdot n\, |\nabla \psi|$ coming from the Hamilton-Jacobi equation, as it is done in [29] and [50], without making any further assumptions. For example, in [21] it is shown that the transported level set function remains the signed distance function (at least for a small time) if the advection velocity remains constant along the normal, namely $(\theta \cdot n)(x) = (\theta \cdot n)(p_\Gamma(x))$.

A difficulty with (42) is that it does not satisfy the Hadamard structure theorem (see e.g. [2], [17], [23], [32] and references therein) since it does not depend solely on the normal trace $\theta \cdot n$ on the interface $\Gamma = \partial\Omega$. In fact, assuming that the support of $\frac{\partial m}{\partial \psi}$ is concentrated around Γ, formula (42) would be similar to what we called earlier approximate shape derivative, obtained in Proposition 2.5 for a discretization of the sharp-interface case and in (29) for the smoothed-interface case when the regularization parameter ε is small. In any case, (42) does not guarantee a descent direction in general, unless $\frac{\partial m}{\partial \psi}$ keeps a constant sign along the normal, at least for the width of the intermediate zone.

6. Numerical results

6.1. Level-set representation.

Following the lead of [4], [5], we represent the moving and optimizable interfaces by level set functions [36] defined on a fixed mesh in an Eulerian framework. According to Section 4, using m level-set functions we can represent up to 2^m separate phases.

When there are only two phases to optimize, it suffices to use one level-set function to represent the interface Γ between two complementary sub-domains Ω^0 and Ω^1 of the working domain D. The level set function ψ (see Figure 7) is defined by

$$\begin{cases} \psi(x) = 0 & \text{for } x \in \Gamma = \partial\Omega_0, \\ \psi(x) < 0 & \text{for } x \in \Omega^0, \\ \psi(x) > 0 & \text{for } x \in \Omega^1. \end{cases}$$
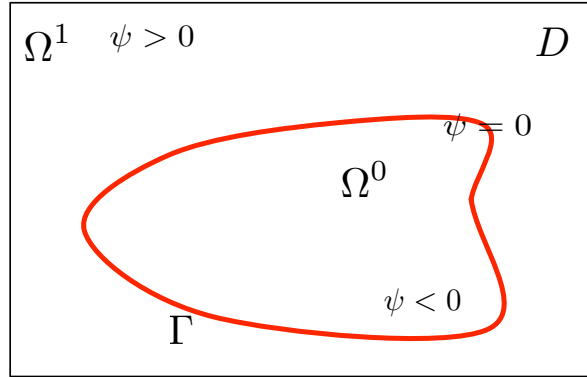

FIGURE 7. Level-set representation of the domains Ω^0 and Ω^1.

During the optimization process the shape is advected with a scalar velocity field $V(x)$ in the direction of the outer normal vector field $n(x)$ to Ω^0 ($V = \theta \cdot n$). According to section 3, the value of this scalar field is derived from the shape sensitivity analysis of Theorem 3.14. More precisely, the choice

$$V(x) = f_0(x) + f_1(x),$$

where f_0, f_1 are defined by (25), clearly gives a descent direction for $\theta = V n$. The functions f_0 and f_1 are defined for all points $x \in \Gamma$ as integrals along rays in the normal direction. Since the interface Γ is not explicitly discretized, f_0 and f_1 are evaluated at the nodes of the elements that are crossed by the zero level-set. The normal vector is computed for each of these nodes, which defines the direction of the rays and a simple quadrature formula is used for the numerical approximation of f_0 and f_1. This computation is done only in a band of thickness 2ε around the interface, where h'_ε is non-zero, and as long as the skeleton (see Definition 3.3) is not detected (recall that the rays end up at the skeleton). When integrating along a ray the skeleton is identified as soon as the signed-distance function looses its monotonicity.

The advection is described in the level set framework by introducing a pseudo time $t \in \mathbb{R}_+$ and solving the Hamilton-Jacobi equation over D

$$\frac{\partial \psi}{\partial t} + V|\nabla \psi| = 0, \tag{43}$$

using an explicit upwind scheme [39]. However, the scalar field V is a priori defined only on the boundary of the shape and therefore it is necessary to extend it to the whole domain in order to be able to perform multiple iterations of the transport equation (43) for each finite element analysis. Moreover, it is numerically advantageous to regularize the advection velocity in order to assure some smoothness required by sensitivity analysis [15]. One way to extend and regularize at the same time V is to solve the variational formulation for $Q \in H^1(D)$

$$\int_D \left(\alpha^2 \nabla Q \cdot \nabla V + Q V \right) dx = J'(\Omega)(V n) \quad \text{for any } V \in H^1(D), \tag{44}$$

where $\alpha > 0$ is a positive parameter that controls the regularization width (typically α is of the order of the mesh size). Then, choosing $V = -Q$, we find

$$J'(\Omega)(-Q n) = -\int_D \left(\alpha^2 |\nabla Q|^2 + Q^2 \right) dx,$$

which guarantees again a descent direction for J.

In order to describe up to four distinct phases, two level-set functions ψ_0 and ψ_1 are defined such that

$$\left\{ \begin{array}{ll} \psi_0(x) = 0 & \text{for } x \in \partial\mathcal{O}^0, \\ \psi_0(x) < 0 & \text{for } x \in \mathcal{O}^0, \\ \psi_0(x) > 0 & \text{for } x \in {}^c\overline{\mathcal{O}^0}, \end{array} \right. \quad \text{and} \quad \left\{ \begin{array}{ll} \psi_1(x) = 0 & \text{for } x \in \partial\mathcal{O}^1, \\ \psi_1(x) < 0 & \text{for } x \in \mathcal{O}^1, \\ \psi_1(x) > 0 & \text{for } x \in {}^c\overline{\mathcal{O}^1}, \end{array} \right.$$

following the notations of Figure 4. Then, each level-set function ψ_i, $i = 0, 1$, is transported independently solving (43), where V_i, $i = 0, 1$ results from the formulas (38) and (39).

FIGURE 8. Boundary conditions for the long cantilever.

6.2. **Two materials in the sharp interface context.**

We work in the context of Section 2, namely in a sharp interface framework. We compare the two shape derivatives: the continuous formula furnished by Proposition 2.2 and the discrete formula given in Proposition 2.5. The numerical implementation of the continuous formula of the shape derivative in Proposition 2.2 is achieved according to the scheme proposed in [5] for computing the jump approximation (12). We consider a long cantilever of dimensions 2×1, discretized by 100×50 $P1$ elements, clamped at its left side and submitted to a unit vertical load at the middle of its right side (see Figure 8). The domain is filled by two isotropic materials 0 and 1, with different Young's moduli, respectively $E^0 = 0.5$ and $E^1 = 1$ (material 1 is stiffer than material 0) but with the same Poisson ratio $\nu = 0.3$. We minimize the compliance (3) with a constraint of fixed volume for the two phases. The computations are done with the FreeFem++ package [38].

For all the numerical examples in this paper, an augmented Lagrangian method is applied to handle the constraints. Following the approach in [33], supposing that our problem contains m equality constraints of the type $c_i(\Omega^0) = 0$ $(i = 1, ..., m)$, an augmented Lagragian function is constructed as

$$L(\Omega^0, \ell, \mu) = J(\Omega^0) - \sum_{i=1}^{m} \ell_i c_i(\Omega^0) + \frac{\mu_i}{2} \sum_{i=1}^{m} c_i^2(\Omega^0),$$

where $\ell = (\ell_i)_{i=1,...,m}$ and $\mu = (\mu_i)_{i=1,...,m}$ are Lagrange multipliers and penalty parameters for the constraints. The Lagrange multipliers are updated at each iteration n according to the optimality condition $\ell_i^{n+1} = \ell_i^n - \mu_i c_i(\Omega_n^0)$. The penalty parameters are augmented every 5 iterations. With such an algorithm the constraints are enforced only at convergence (see for example Figure 10). Of course, other (and possibly more efficient) optimization algorithms could be used instead.

The results are displayed on Figure 9. As usual the strong phase 1 is black and the weak phase 0 is white. The design obtained with the discrete formula is quite similar to the one exposed in Figure 11 (c). However the continuous formula gives a different optimal shape which is worse in terms of the objective function than the one obtained with the discrete formula (see Figure 10).
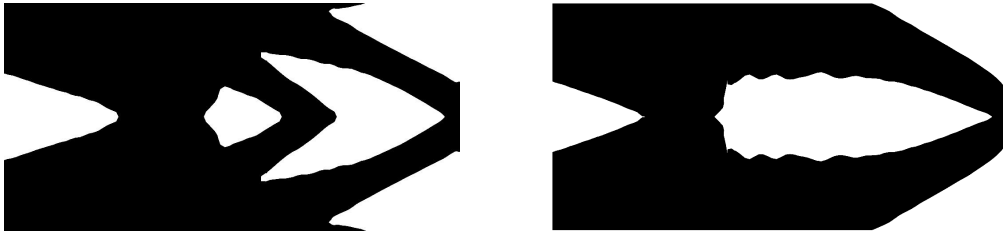

FIGURE 9. Optimal shapes for the long cantilever using the discrete shape gradient (left) and the continuous formula (right).

6.3. **Two materials in the smoothed-interface context.**

We now switch to the smoothed-interface setting as described in Section 3. We perform the same test case, with the same parameter values, as in Section 6.2. All computations are performed in Scilab. A first goal is to compare the smoothed-interface approach to the sharp-interface one. A second goal is to compare the various formulas for the shape derivative obtained in Section 3.

We minimize again the compliance (3) with a constraint of fixed volume for the two phases which is written

$$\int_D h_\varepsilon(d_{\Omega^0}(x))dx = V_T,$$

where V_T is the target volume of the strong phase occupying Ω^1.

We test three different formulas for the shape gradient. The first one is the "true" formula given by (25) (see also (38) and (39) in the case of more than two phases). The second one, called "Jacobian-free", is
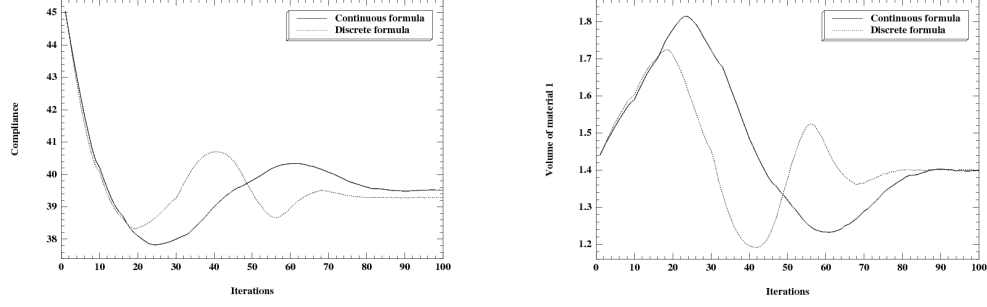
FIGURE 10. Convergence history of the compliance (left) and the volume (right) for the sharp interface results displayed on Figure 9.
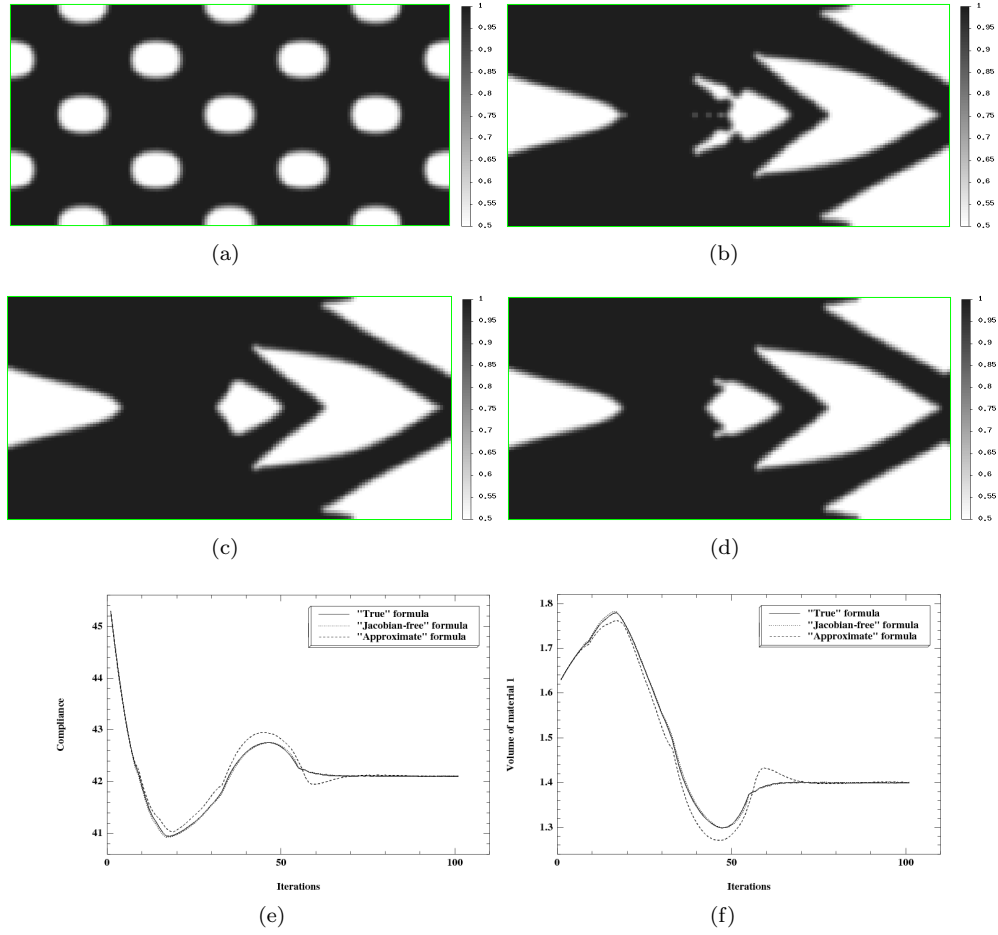

(a)

(b)

(c)

(d)

(e)

(f)

FIGURE 11. *Long cantilever using two phases with $V_T = 0.7|D|$ and a small smoothing parameter $\varepsilon = 2\Delta x$; (a) initialization, (b) optimized shape using the "true" formula, (c) optimized shape using the "Jacobian-free" formula, (d) optimized shape using the "approximate" formula, (e) convergence of the compliance, (f) convergence of the volume.*

(28) which is obtained from (25) by neglecting the Jacobian term (see Remark 3.10). The reason for this choice is that the curvature is not precisely calculated using a fixed mesh and therefore we may introduce a significant approximation error. In any case, it amounts to neglecting a positive factor, thus it remains a

descent direction. The third one is the "approximate" formula (29) obtained for a very thin smoothing zone around the interface.

First, we consider the case of a "thin" interface. The interpolation width is chosen as $\varepsilon = 2\Delta x$, where Δx is the uniform mesh size. The results for $V_T = 0.7|D|$ are shown in Figure 11. We plot the Young modulus distribution (black being the strong material A_1 and white the weak material A_0). The convergence histories are almost identical for the "true" and "Jacobian-free" formulas of the shape derivative. It is slightly more oscillating for the "approximate" formula although it converges to almost the same value of the objective function. The resulting optimal designs are very similar.

For a larger interpolation width $\varepsilon = 8\Delta x$ ("thick" interface), the results are shown in Figure 12. We clearly see a difference for the optimal shape obtained using the "true" formula of the shape derivative: in this case, the algorithm produces a very long and oscillating interface in such a way that the overall structure is almost like a composite structure. This is due to the fact that the intermediate zone inside the interface is very favorable compared to the pure phases. Nevertheless, despite the differences in the final shapes, the values of the compliance are almost the same for the "true" and "Jacobian-free" formulas, slightly worse for the "approximate" formula of the shape gradient.
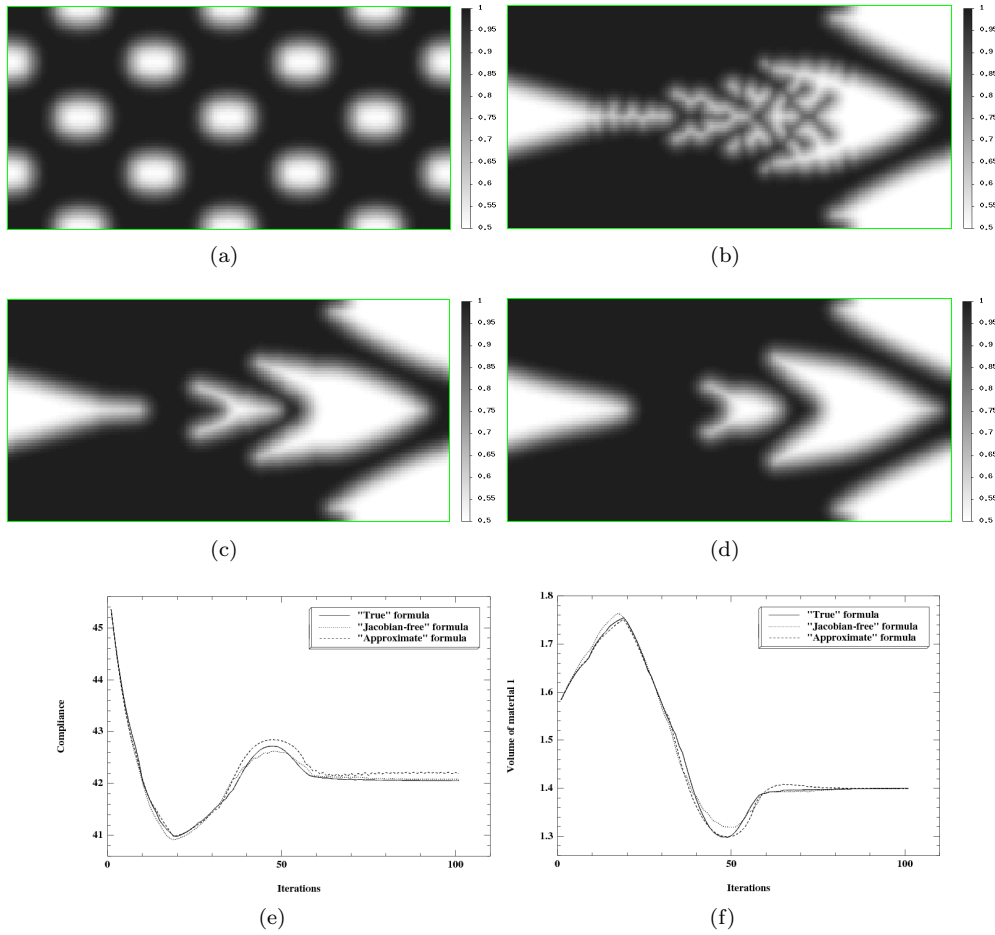

FIGURE 12. *Long cantilever using two phases with $V_T = 0.7|D|$ and a large smoothing parameter $\varepsilon = 8\Delta x$; (a) initialization, (b) optimized shape using the "true" formula, (c) optimized shape using the "Jacobian-free" formula, (d) optimized shape using the "approximate" formula, (e) convergence of the compliance, (f) convergence of the volume.*

6.4. **Four phases in the smoothed interface context.**

We consider now the case of using up to four phases and consequently two level-set functions. A smoothed approximation of the characteristic function of each phase can be constructed using combinations of the functions h_ε, defined in equation (16), as follows

$$
(45) \quad
\begin{cases}
\chi_0 = (1 - h_\varepsilon(d_{\mathcal{O}^0}))(1 - h_\varepsilon(d_{\mathcal{O}^1})), \\
\chi_1 = h_\varepsilon(d_{\mathcal{O}^0})(1 - h_\varepsilon(d_{\mathcal{O}^1})), \\
\chi_2 = (1 - h_\varepsilon(d_{\mathcal{O}^0}))h_\varepsilon(d_{\mathcal{O}^1}), \\
\chi_3 = h_\varepsilon(d_{\mathcal{O}^0})h_\varepsilon(d_{\mathcal{O}^1}),
\end{cases}
$$

and the global Hooke's tensor in given by (35). The optimization problem now reads

$$
(46) \quad
\begin{aligned}
\min_{\mathcal{O}^0,\mathcal{O}^1 \in \mathcal{U}_{ad}} J(\mathcal{O}^0,\mathcal{O}^1) &= \int_D A_{\mathcal{O}^0,\mathcal{O}^1,\varepsilon}(x)e(u) : e(u)\, dx \\
\text{s.t.} \quad \int_D \chi_i dx &= V_T^i,\ i = 0,...,3\,,
\end{aligned}
$$

where V_T^i is the target volume for the phase i (they sum up to the volume of D). As previously, an augmented Lagrangian algorithm is applied to enforce the constraints. In this section we wrok with a "thin" interface, namely $\varepsilon = 2\Delta x$. For all test cases, we checked numerically that the three formulas of the shape gradient give very similar optimal shapes, as expected. The results presented in the sequel have been obtained using the "Jacobian-free" formula.

We test our method with several benchmark examples presented in [50] and [51]. Since the initial design are different, as well as the numerical methods, it is hard to make a quantitative comparison and we satisfy ourselves with a qualitative comparison.

6.4.1. *Short cantilever using two materials and void.*

In this paragraph we consider only three phases, made of two materials and void. The first structure to be optimized is a two-dimensional short cantilever, of dimensions 1×2, discretized using 80×160 $Q1$ elements. The left part of the structure is clamped and a unitary vertical force is applied at the mid point of its right part (see Figure 13). The Young moduli of the four phases are defined as $E^0 = 0.5, E^1 = 10^{-3}, E^2 = 1$ and $E^3 = 10^{-3}$, where both phases 1 and 3 represent void. The target volumes for phases 0 and 2 are set to $V_T^0 = 0.2|D|$ and $V_T^2 = 0.1|D|$. Remark that phases 1 and 3 are the same, corresponding to void. The fact that the void zone is represented by two different characteristic functions has no influence on the numerical results (at least in all our numerical experiments). The initial and the optimal shape (obtained after 200 iterations) are shown in Figure 14 (a) and (b). We plot the Young modulus with a grey scale: dark stands for the stronger phase, white for void and grey for the intermediate phase.

This test case was previously studied in [50] (see figures 7 and 8 therein for two different initializations). Our results are roughly similar to those in [50] and even slightly better since the design of Figure 14 (b) is symmetric (as expected), contrary to the results in [50].

6.4.2. *Short cantilever using three materials and void.*

The same example as in the previous paragraph is considered here with an additional phase: half of the volume of material 0 is replaced by a weaker material 1. More precisely, the Young moduli of the four phases are defined as $E^0 = 0.5, E^1 = 0.25, E^2 = 1$ and $E^3 = 10^{-3}$, while the target volumes for the three materials 0, 1 and 2 are set to $V_T^0 = V_T^1 = V_T^2 = 0.1|D|$. The initial and optimal shapes (after 200 iterations) are displayed on Figure 14 (c) and (d).

This test case was also studied in [50] (see figures 11 and 12 therein for two different initializations). Our result differs notably from these previous ones. Indeed, in [50] the strong material 2 always forms a two-bar truss which is further reinforced by the other materials. On the contrary, in our Figure 14 (d) the strong phase is disconnected and the intermediate material 0 plays a more active role in the transfer of the load to the fixed wall.
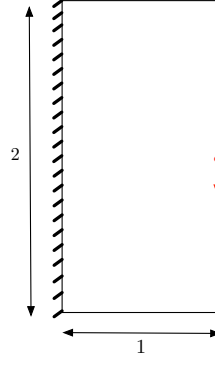
FIGURE 13. Boundary conditions and initialization for the short cantilever.
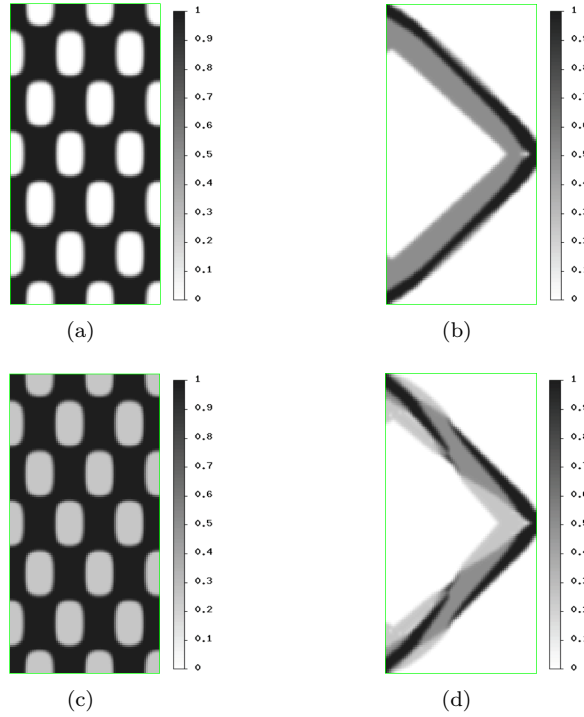

(a)

(b)

(c)

(d)

FIGURE 14. *Short cantilever using two or three phases and void; (a) initialization for two phases and void, (b) optimal shape for two phases and void, (c) initialization for three phases and void, (d) optimal shape for three phases and void.*

6.4.3. *3-force bridge using two materials and void.*

A bridge-type structure of dimensions 2×1 is discretized by 160×80 $Q1$ elements. Both the horizontal and vertical displacement are fixed at the lower left part as well as the vertical displacement of the lower right part. Three equally spaced forces are applied at the lower part (see Figure 15). The value of F is set to 1. The Young moduli of the four phases are set to $E^0 = 0.5, E^1 = 10^{-3}, E^2 = 1$ and $E^3 = 10^{-3}$ and the target volumes for phases 0 and 2 are set to $V_T^0 = 0.2|D|$ and $V_T^2 = 0.1|D|$. The initial and optimal designs (after 250 iterations) are shown in Figure 16 (a) and (b).

Once again this test case was performed in [50] (see figure 13 therein). Our result is quite different. First, our design in Figure 16 (b) is symmetric, as it should be. Second, a major difference occurs in the use of the

strong phase. In our design, the strong material is used in the lower part of the "radial" bars whereas it was absent in figure 13 of [50] (and rather used in the upper "arch").
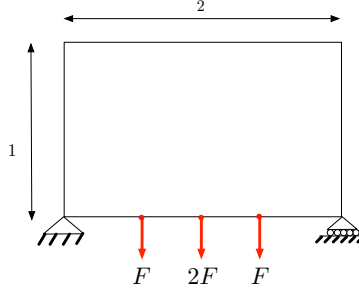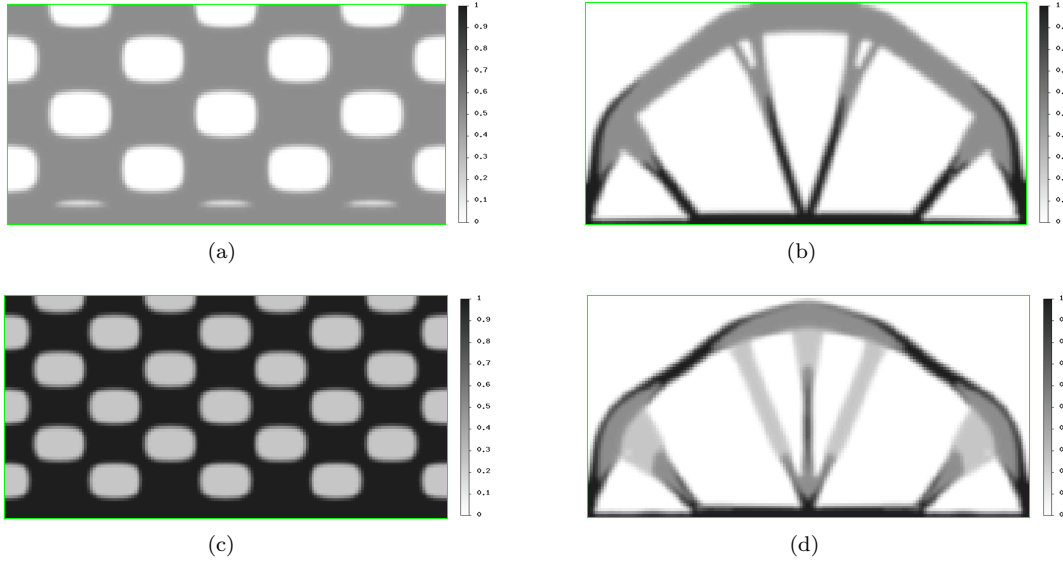

FIGURE 15. Boundary conditions for the 3-force bridge.

(a)

(b)

(c)

(d)

FIGURE 16. *3-force bridge using two or three phases and void; (a) initialization for two phases and void, (b) optimal shape for two phases and void, (c) initialization for three phases and void, (d) optimal shape for three phases and void.*

6.4.4. *3-force bridge using three materials and void.*

The same example as in the previous paragraph is considered here with an additional phase: half of the volume of material 0 is replaced by a weaker material 1. The Young moduli of the four phases are defined as $E^0 = 0.5, E^1 = 0.25, E^2 = 1$ and $E^3 = 10^{-3}$, while the target volumes for phases 0, 1 and 2 are set to $V_T^0 = V_T^1 = V_T^2 = 0.1|D|$. The initial and optimal designs (after 250 iterations) are displayed on Figure 14 (c) and (d).

This test case can be found in [50] (figure 14) too, and again our result is quite different.

6.4.5. *Medium cantilever using three materials and void.*

The next structure is a medium cantilever of dimensions 3.2×2, discretized using 120×75 $Q1$ elements. The left part of the structure is clamped and a unitary vertical force is applied at the bottom of its right

part (see Figure 17). The Young moduli of the four phases are again set to $E^0 = 0.5, E^1 = 0.25, E^2 = 1$ and $E^3 = 10^{-3}$, while the target volumes for phases 0, 1 and 2 are $V_T^0 = V_T^1 = V_T^2 = 0.1|D|$. The initial and optimal shapes (after 250 iterations) are shown in Figure 18.

This test case was also performed in [51] (see figure 7 therein). Our optimal design has a more complex topology and a different layout of the three materials. However, the final volumes of the three materials in [51] are not the same as ours and thus a comparison is not easy to establish.
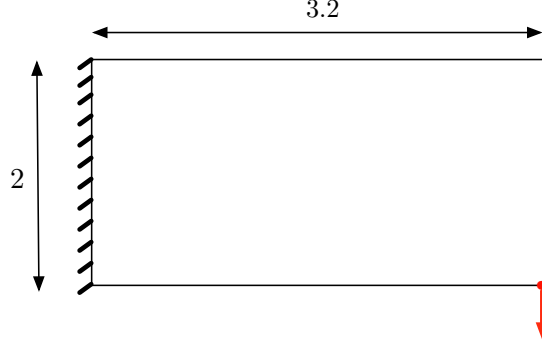

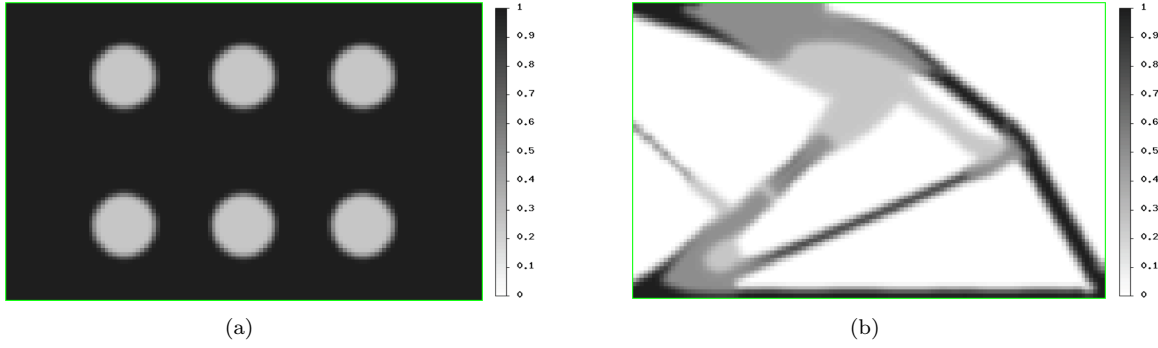FIGURE 17. Boundary conditions and initialization for the medium cantilever.

FIGURE 18. *Medium cantilever using three materials and void; (a) initialization, (b) optimal shape.*

6.4.6. *Long cantilever using two materials and void.*

The goal of this last paragraph is twofold. First, we consider again the 2×1 long cantilever, as in Figure 8, but with four phases, defined by their Young moduli $E^0 = 0.5, E^1 = 10^{-3}, E^2 = 1$ and $E^3 = 10^{-3}$. Second, we switch to an unconstrained optimization algorithm. We do not impose equality constraints for the volume of each phase. Rather, we fix Lagrange multipliers and we minimize an objective function $J(\mathcal{O}^0, \mathcal{O}^1)$, which reads

$$(47) \qquad J(\mathcal{O}^0, \mathcal{O}^1) = \int_D A(d_{\mathcal{O}^0}, d_{\mathcal{O}^1})e(u) : e(u)dx + \sum_{i=0}^{3} \ell^i \int_D \chi_i(x)dx.$$

We then carry out a standard constraint-free steepest descent algorithm in order to minimize J.

A small tolerance parameter $tol > 0$ (in the example below, we used $tol = 0.02$) over acceptance of the produced shapes is introduced so as to ease the occurrence of topological changes and is then turned off after some iterations. More accurately, in the course of the optimization process, a step $\mathcal{O}_n^0 \to \mathcal{O}_{n+1}^0$ and $\mathcal{O}_n^1 \to \mathcal{O}_{n+1}^1$ is accepted provided:

$$J(\mathcal{O}_{n+1}^0, \mathcal{O}_{n+1}^1) < (1 + tol)J(\mathcal{O}_n^0, \mathcal{O}_n^1).$$
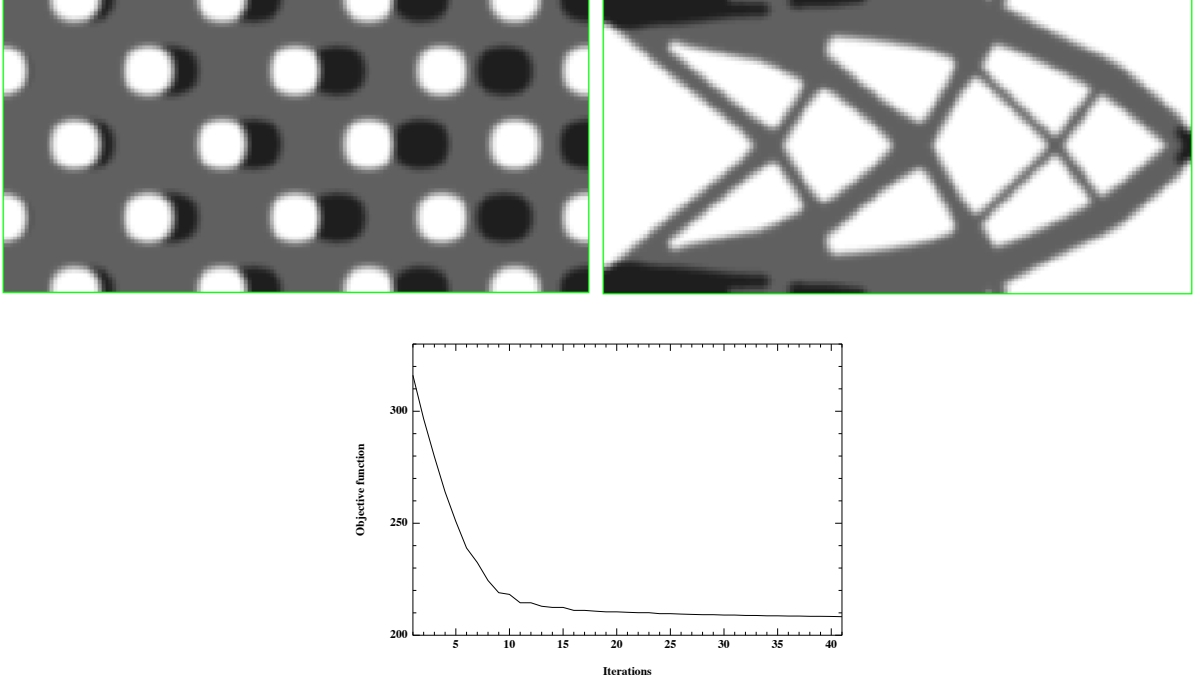
FIGURE 19. Initialization with two materials (top left), optimial shape (top right) and convergence history of the objective function (bottom).

For the results shown in Figure 19, the Lagrange multipliers in (47) are set to $\ell^0 = 100, \ell^1 = 0, \ell^2 = 200, \ell^3 = 0$. As can be expected the strong material is distributed at the areas of high stress, while the weak material completes the shape of the optimal cantilever.

It is interesting to see the optimal subdomains $\mathcal{O}^0$ and $\mathcal{O}^1$ (defined in Section 4) in Figure 20. Recall that it is the intersections of these two subdomains and their complementaries which give rise to the phase domains in the optimal design of Figure 19. Nevertheless, $\mathcal{O}^0$ and $\mathcal{O}^1$ are important from a numerical point since, rather than the phase domains, they are advected by the shape gradients and represented by the level set functions.

FIGURE 20. Final subdomains $\mathcal{O}^0$ (left) and $\mathcal{O}^1$ (right).

References

[1] G. Allaire, *Shape optimization by the homogenization method, Springer Verlag, New York* (2001).

[2] G. Allaire, *Conception optimale de structures*, Mathématiques et Applications 58, Springer, Heidelberg (2006).

[3] G. Allaire, C. Castro, *A new approach for the optimal distribution of assemblies in a nuclear reactor,* Numerische Mathematik, 89, pp.1-29 (2001).

[4] G. Allaire and F. Jouve and A.M. Toader, *Structural optimization using shape sensitivity analysis and a level-set method*, J. Comput. Phys., 194 (2004) pp. 363–393.

[5] G. Allaire, F. Jouve and N. Van Goethem, *Damage evolution in brittle materials by shape and topological sensitivity analysis,* J. Comput. Phys., 230 (2011) pp. 5010–5044.

[6] L. Ambrosio, *Lecture notes on geometric evolution problems, distance function and viscosity solutions,* in Calculus of Variations and Partial Differential Equations, G. Buttazo, A. Marino, M.K.V. Murthy Eds, Springer, 5-93 (1999).

[7] M. Bendsoe, O. Sigmund, *Topology Optimization. Theory, Methods, and Applications*, Springer Verlag, New York (2003).

[8] Ch. Bernardi, O. Pironneau, *Sensitivity of Darcy's law to discontinuities*, Chinese Ann. Math. Ser. B **24**, no. 2, pp.205-214 (2003).

[9] H.-J. Butt, K. Graf, M. Kappl, *Physics and Chemistry of Interfaces*, Wiley (2003).

[10] P. Cannarsa and P. Cardaliaguet, *Representation of equilibrium solutions to the table problem for growing sandpiles*, J. Eur. Math. Soc. 6 (2004), pp. 1–30.

[11] J. Céa, *Conception optimale ou identification de formes, calcul rapide de la dérivée directionnelle de la fonction coût*, Math. Model. Num. 20, 3 (1986), pp. 371–420.

[12] I. Chavel, *Riemannian Geometry, a modern introduction*, 2nd Edition, Cambridge University Press (2006).

[13] A. Cherkaev, *Variational Methods for Structural Optimization*, Springer, New York (2000).

[14] C. Dapogny, *Ph.D. thesis*, Université Pierre et Marie Curie. In preparation.

[15] F. de Gournay, *Velocity extension for the level-set method and multiple eigenvalues in shape optimization.* SIAM J. on Control and Optim., 45, no. 1, 343–367 (2006).

[16] G. Delgado, *Ph.D. thesis*, Ecole Polytechnique. In preparation.

[17] M.C. Delfour and J.-P. Zolesio, *Shapes and Geometries: Metrics, Analysis, Differential Calculus, and Optimization*, SIAM, Philadelphia 2nd ed. (2011).

[18] M. C. Delfour and J.-P. Zolesio, *Shape identification via metrics constructed from the oriented distance function*, Control and Cybernetics 34, No 1 (2005) pp. 137-164.

[19] L. C. Evans and R. F. Gariepy, *Measure theory and fine properties of functions*, CRC Press (1992).

[20] H. Federer, *Curvature Measures*, Transactions of the American Mathematical Society Vol. 93, No. 3 (1959), pp. 418-491.

[21] J. Gomes and O. Faugeras, *Reconciling distance functions and level sets*, Scale-Space Theories in Computer Vision, pp. 70-81, Springer (1999).

[22] J. Haslinger, J. Dvorak, *Optimum composite material design,* RAIRO M2AN, 29, pp.657-686 (1995).

[23] A. Henrot and M. Pierre, *Variation et optimisation de formes, une analyse géométrique*, Mathématiques et Applications 48, Springer, Heidelberg (2005).

[24] F. Hettlich, W. Rundell, *The determination of a discontinuity in a conductivity from a single boundary measurement*, Inverse Problems, **14**, no. 1, pp.67-82 (1998).

[25] A.L. Karchevsky, *Reconstruction of pressure velocities and boundaries of thin layers in thinly-stratified layers*, J. Inverse Ill-Posed Probl. 18 (2010), no. 4, 371-388.

[26] R. Lipton, *Design of functionally graded composite structures in the presence of stress constraints*, Internat. J. Solids Structures 39 (2002), no. 9, 2575-2586.

[27] C. Mantegazza and A.C. Menucci, *Hamilton-Jacobi Equations and Distance Functions on Riemannian Manifolds*, Applied Math. and Optim., vol 47, (2002), pp. 1-25.

[28] W. Mc Lean, *Strongly Elliptic Systems and Boundary Integral Equations*, Cambridge University Press, Cambridge (2000).

[29] Y. Mei and X. Wang, *A level set method for structural topology optimization with multi-constraints and multi-materials,* Acta Mechanica Sinica, Vol.20, No.5, (2004).

[30] Y. Mei and X. Wang, *A level set method for structural topology optimization and its applications,* Advances in Engineering software, Vol.35, 415-441 (2004).

[31] G. Milton, *The theory of composites,* Cambridge University Press (2001).

[32] F. Murat and J. Simon, *Sur le contrôle par un domaine géométrique*, Technical Report RR-76015, Laboratoire d'Analyse Numérique (1976).

[33] J. Nocedal, S.J. Wright, *Numerical optimization.* Springer Science+ Business Media (2006).

[34] Zh.O. Oralbekova, K.T. Iskakov, A.L. Karchevsky, *Existence of the residual functional derivative with respect to a coordinate of gap point of medium*, to appear in Appl. Comput. Math.

[35] J.M. Ortega and W.C. Rheinboldt, *On discretization and differentiation of operators with application to Newton's method*, SIAM journal on numerical analysis, 3,1, 143-156 (1966).

[36] S. J. Osher and J.A. Sethian, *Front propagating with curvature dependent speed: algorithms based on Hamilton-Jacobi formulations,* J. Comp. Phys. **78** (1988) pp. 12-49

[37] O. Pantz, *Sensibilité de l'équation de la chaleur aux sauts de conductivité*, C. R. Acad. Sci. Paris, Ser. I 341 pp.333-337 (2005).

[38] O. Pironneau, F. Hecht, A. Le Hyaric, *FreeFem++ version 2.15-1*, http://www.freefem.org/ff++/.

[39] J.A. SETHIAN, *Level-Set Methods and fast marching methods: evolving interfaces in computational geometry, fluid mechanics, computer vision and materials science,* Cambridge University Press (1999).

[40] O. SIGMUND AND S. TORQUATO, *Design of materials with extreme thermal expansion using a three-phase topology optimization method*, Journal of the Mechanics and Physics of Solids, 45(6):1037-1067 (1997).

[41] O. SIGMUND, *Design of multiphysics actuators using topology optimization-part ii: Two-material structures*, Computer methods in applied mechanics and engineering, 190(49):6605-6627 (2001).

[42] N. SUKUMAR, D.L. CHOPP, N. MOES AND T. BELYTSCHKO, *Modeling holes and inclusions by level sets in the extended finite element method* , Comput. Methods Appl. Mech. Engrg., 190, (2001), 6183-6200.

[43] S. SURESH, A. MORTENSEN, *Fundamentals of functionally graded materials*, London: Institute of Materials (1998).

[44] C.C. SWAN, I. KOSAKA, *Voigt-Reuss topology optimization for structures with linear elastic material behaviors*, Int. J. Numer. Methods Engrg. 40 (1997).

[45] L. TARTAR, *The general theory of homogenization. A personalized introduction*, Lecture Notes of the Unione Matematica Italiana, 7. Springer-Verlag, Berlin; UMI, Bologna (2009).

[46] R. TILLEY, *Understanding Solids: The Science of Materials*, Wiley (2004).

[47] N. VERMAAK, G. MICHAILIDIS, Y. BRECHET, G. ALLAIRE, G. PARRY AND R. ESTEVEZ, *Material Interface Effects on the Topology Optimization of Multi-Phase Thermoelastic Structures Using A Level Set Method*, In preparation.

[48] L.A. VESE AND T.F. CHAN, *A multiphase level set framework for image segmentation using the Mumford and Shah model*, Int. J. Comput. Vision 50 (3) (2002) 271-293.

[49] M. WANG, S. CHEN, X. WANG AND Y. MEI, *Design of Multimaterial Compliant Mechanisms Using Level-Set Methods*, J. Mech. Des. 127(5), 941-956 (2005).

[50] M. WANG AND X. WANG, *Color level sets: a multi-phase method for structural topology optimization with multiple materials*, Comput. Methods Appl. Mech. Engrg. 193, 469-496 (2004).

[51] M. WANG AND X. WANG, *A level-set based variational method for design and optimization of heterogeneous objetcs*, Compututer-Aided Design 37, 321-337 (2005).

[52] L. YIN AND G.K. ANANTHASURESH, *Topology optimization of compliant mechanisms with multiple materials using a peak function material interpolation scheme*, Struct. Multidiscip. Optim. 23, 49-62 (2001).

[53] S. ZHOU AND Q. LI, *Computational design of multi-phase microstructural materials for extremal conductivity*, Computational Materials Science, 43:549-564 (2008).

[54] S. ZHOU AND M.Y. WANG, *Multimaterial structural optimization with a generalized Cahn-Hilliard model of multiphase transition*, Struct. Multidisc. Optim. 33:89-111 (2007).